Journal of Geochemical Exploration 196 (2019) 192–207

Contents lists available at ScienceDirect

Journal of Geochemical Exploration

journal homepage: www.elsevier.com/locate/gexplo

# Geochemistry of Palaeogene coals from the Fuqiang Mine, Hunchun Coalfield, northeastern China: Composition, provenance, and relation to the adjacent polymetallic deposits

Wenmu Guo[a,b], Shifeng Dai[a,b,c,*], Victor P. Nechaev[d,e], Evgeniya V. Nechaeva[e], Guojun Wei[f], Robert B. Finkelman[g], Baruch F. Spiro[h]

[a] State Key Laboratory of Coal Resources and Safe Mining, China University of Mining and Technology, China
[b] College of Geoscience and Survey Engineering, China University of Mining and Technology, Beijing 100083, China
[c] School of Resources and Geosciences, China University of Mining and Technology, Xuzhou 221116, China
[d] Far East Geological Institute, 159 Pr 100-let Vladivostoku, Vladivostok 690022, Russia
[e] Engineering School, Far Eastern Federal University, 8, Sukhanova Str., Vladivostok 690950, Russia
[f] Mengdong Energy Group Co., Ltd., Xilinhot, Inner Mongolia 026000, China
[g] Geosciences Department, University of Texas at Dallas, Richardson, TX, USA
[h] Department of Mineralogy, Natural History Museum, Cromwell Road, London SW7 5BD, UK

ARTICLE INFO

*Keywords:*
Paleogene coals
Trace elements
Hunchun coal basin
Ore deposits

ABSTRACT

This paper describes the geochemistry of the two Palaeogene coal seams (FQ-23 and FQ-26) from the Fuqiang mine, Hunchun Coalfield, Jilin Province, northeastern China. The samples investigated consist of coal, parting, and roof and floor strata. The two Fuqiang coals are lignite/subbituminous rank and have low sulfur contents (0.13% and 0.16% on average, respectively). In comparison with the average values for common global low-rank coals, the Fuqiang coals are richer in W, Cs, Sb, Pb, Li, V, Ga, and Zr.

The terrigenous components in the Fuqiang coals were derived from the Mesozoic (mostly Lower Cretaceous) and Paleozoic igneous and metamorphic rocks, which are abundant in areas surrounding the Hunchun coal basin. The elevated concentrations of trace elements are attributed to two processes: (1) Contribution of clastic materials derived from mineralized Paleozoic rocks, which also host economical ore deposits of these elements; and (2) Mobilisation and redeposition of these elements by acidic waters, which circulated within the coal basin. The latter is evidenced by enrichment in medium rare earth elements, distinct positive Gd anomalies, and high concentrations of boron in the coals. The overall similarity of the geochemical signatures of the Fuqiang coals and the adjacent Au, Cu and W deposits hosted by the Paleozoic igneous and metamorphic rocks underlying and bordering the Hunchun Basin, indicate that they are genetically linked.

## 1. Introduction

The eastern Hunchun area is located at the junction between the western Pacific continental margin and the eastern Xing'an-Mongolian Orogenic Belt (Cao et al., 2011; Sun et al., 2013; Chen et al., 2017; Yang et al., 2018), and the latter is situated between the North China and Siberian cratons. During the Phanerozoic, a series of intensive and extensive tectonic and magmatic activities associated with mineralization events occurred in this area. For example, numerous ore deposits were discovered in the Hunchun area, including the Late Permian Wudaogou orogenic gold and the Yangjingou hydrothermal vein scheelite deposits; the Cretaceous Xiaoxi'nancha porphyry gold-copper deposit and many medium or small-sized tungsten and gold deposits (Fig. 1; Wu et al., 2000, 2002, 2007, 2011; Zhang et al., 2004; Zhang et al., 2010; Donskaya et al., 2012; Xu et al., 2013; Chen et al., 2014; Chai et al., 2015; Ren et al., 2016; Li, 2017). Nearly one hundred tons of gold and hundreds of thousands tons of tungsten resources have been proven in this mineralized zone (Wang et al., 2009). The Hunchun Coal Basin is also close to South Primorye, Far Eastern Russia (Fig. 1b), an area rich in coal resources and coal-hosted Ge—W deposits (Seredin and Danilcheva, 2001).

The Hunchun Basin is a Paleogene fault bounded graben structure (Wang and Wang, 2004). Its basement consists of a large Hercynian granite intrusion, which invaded the Permian and Jurassic-Early

* Corresponding author at: State Key Laboratory of Coal Resources and Safe Mining, China University of Mining and Technology, China.
*E-mail address:* dsf@cumt.edu.cn (S. Dai).

https://doi.org/10.1016/j.gexplo.2018.10.012
Received 12 July 2018; Received in revised form 6 October 2018; Accepted 27 October 2018
Available online 02 November 2018
0375-6742/ 

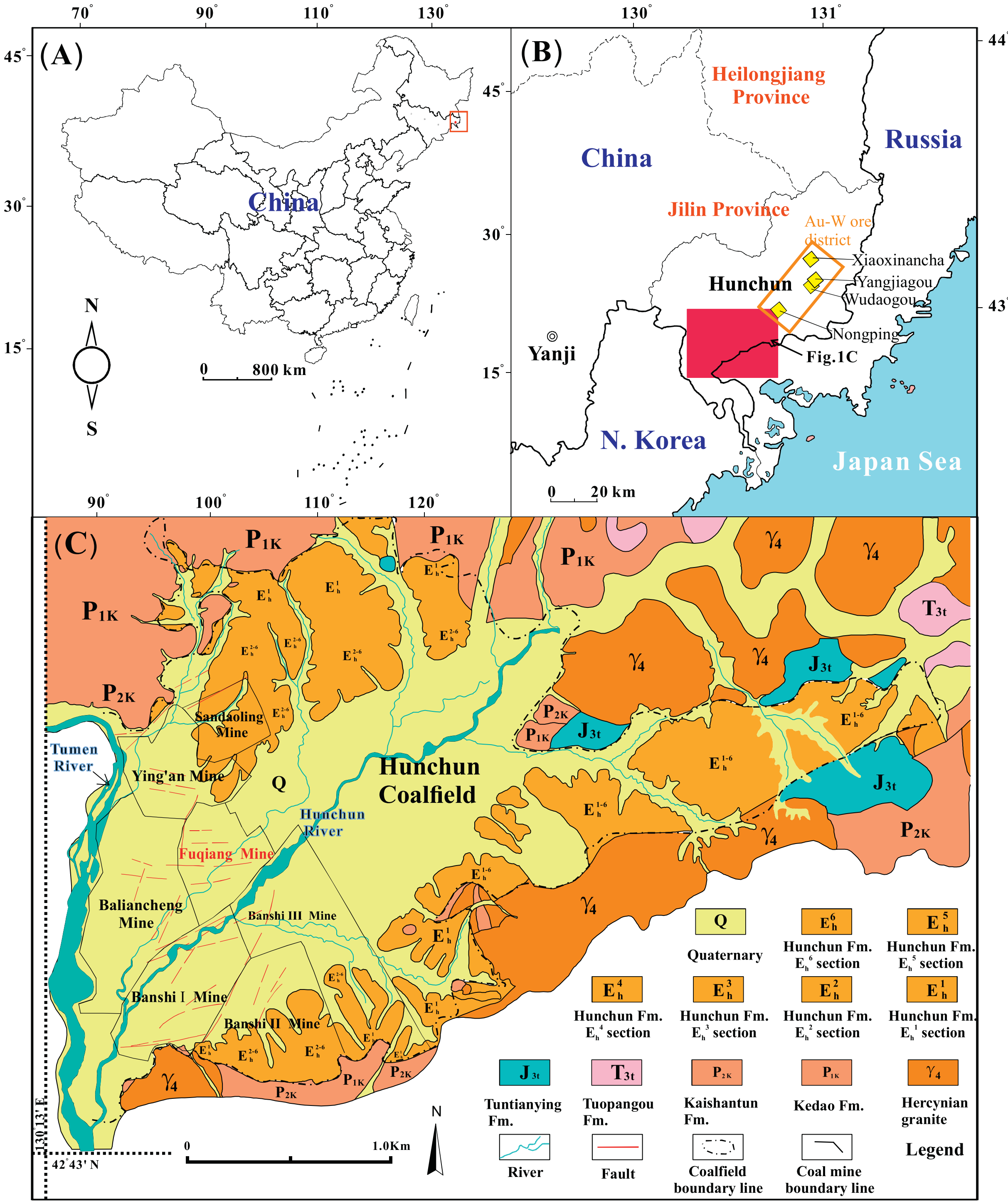


**Fig. 1.** Location of the Hunchun Coalfield and adjacent ore deposits (A, B), coal mines and geological map of the coalfield (C). (A) and (B) are modified after Dai et al. (2018); the locations of ore deposits are from Chen et al. (2017).

Cretaceous volcanic and sedimentary rocks (Xu et al., 2013; Chen et al., 2017; Wang and Wang, 2004). Some Middle Paleozoic metamorphic rocks also occur in the area (Chen et al., 2015). Previous studies focused on metallogenesis, petrology and geochronology of metal ore deposits hosted by rocks in the area (e.g., Zhang et al., 2006; Sun et al., 2008; Zhao et al., 2010; Ren et al., 2012, 2016; Zhao et al., 2013; Chai et al., 2015; Chen et al., 2015, 2017). A total of 25 mineable and non-mineable coal seams were identified in the Hunchun Coalfield (Wang and Wang, 2004). However, to date, there have been only a few reports on coal-bearing sequences in the Hunchun Basin (e.g., Sun, 2015; Wang, 2015) and environmental issues caused by coal combustion (Moon et al., 2000). A recent study by Dai et al. (2018) investigated the modes of occurrence and the source of mineral matter contained in the Palaeogene coal seam and its enclosed intra-seam tonstein in the Baliancheng Mine, near the Fuquian mine of the Hunchun Coalfield (Fig. 1C). There are still two unanswered questions related to geochemical compositions of the coals in this coalfield: 1) Are the sediment source regions of the terrigenous matter of the Fuqiang coals the same as for the coals in the nearby Baliancheng Mine described by Dai et al. (2018)? 2) Are the elevated concentrations of trace elements in the Hunchun coals

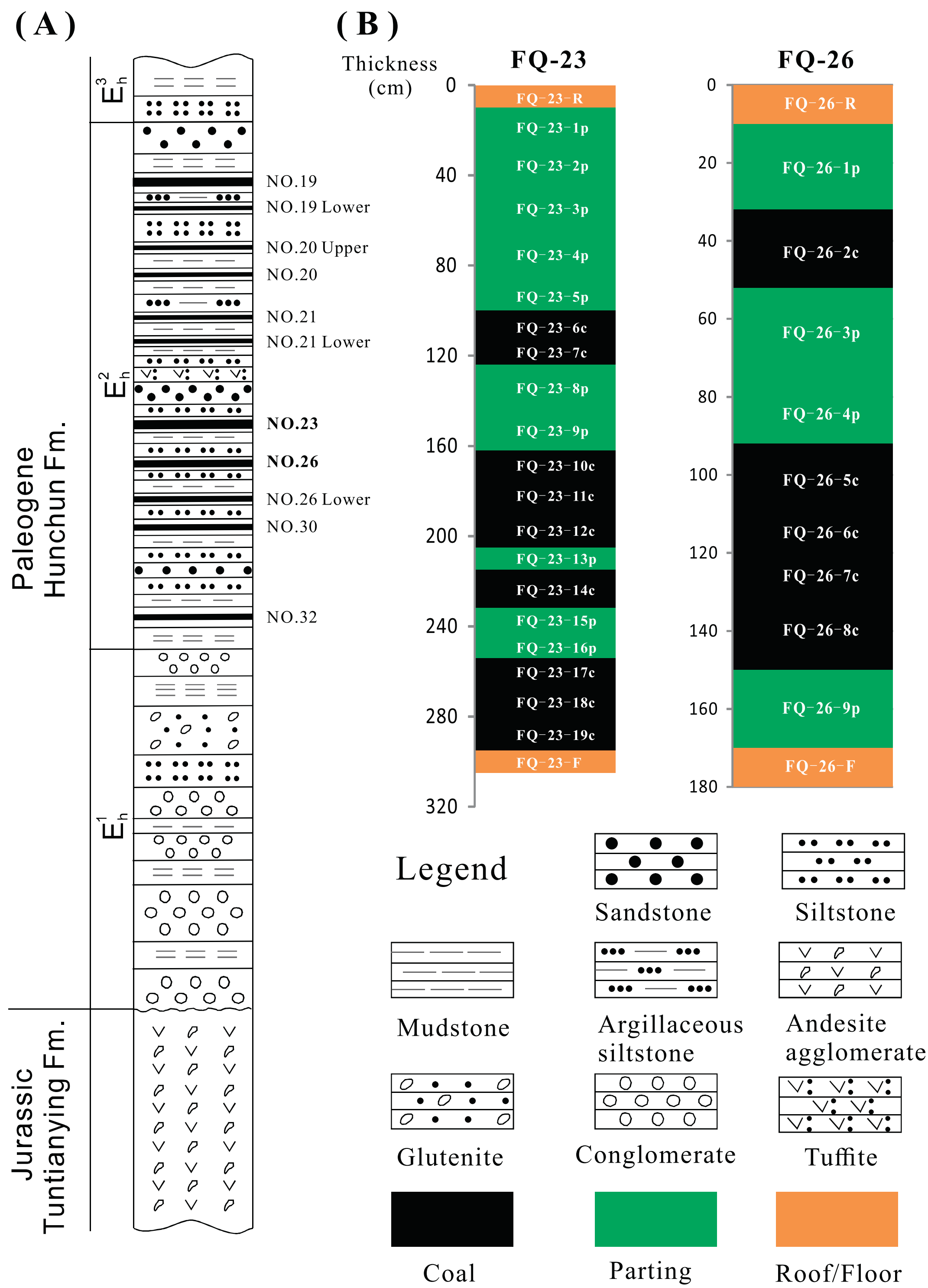


**Fig. 2.** Sedimentary sequences in the Fuqiang mine (A) and the sections of the Nos. 23 and 26 coal seams.

genetically related to polymetallic deposits in the areas surrounding the Hunchum Basin?

In this paper, we report the results of our investigation of the geochemistry of the currently mined Nos. 23 and 26 coal seams (including their roof, partings, and floor horizons) in the Fuqiang Mine in the Hunchun Coalfield. We also discuss genetic relationships between the coals and the adjacent ore deposits with the aim of testing the idea that these coals have the characteristics of 'coal-hosted rare-metal deposits' (Dai et al., 2016a) or 'metalliferous coal' (Seredin and Finkelman, 2008; Dai and Finkelman, 2018), which represents coals with concentrations of critical elements generally over 10-times higher than the averages of corresponding elements in the world coals (Seredin and Finkelman, 2008).

## 2. Geological setting

The geological setting of the Hunchun Coalfield was previously described by Dai et al. (2018). The coalfield is situated in the eastern part of Jilin Province, Northeast China (Fig. 1), covering the area of ~460 $km^2$ between longitudes 130°13′–130°46′E and latitudes

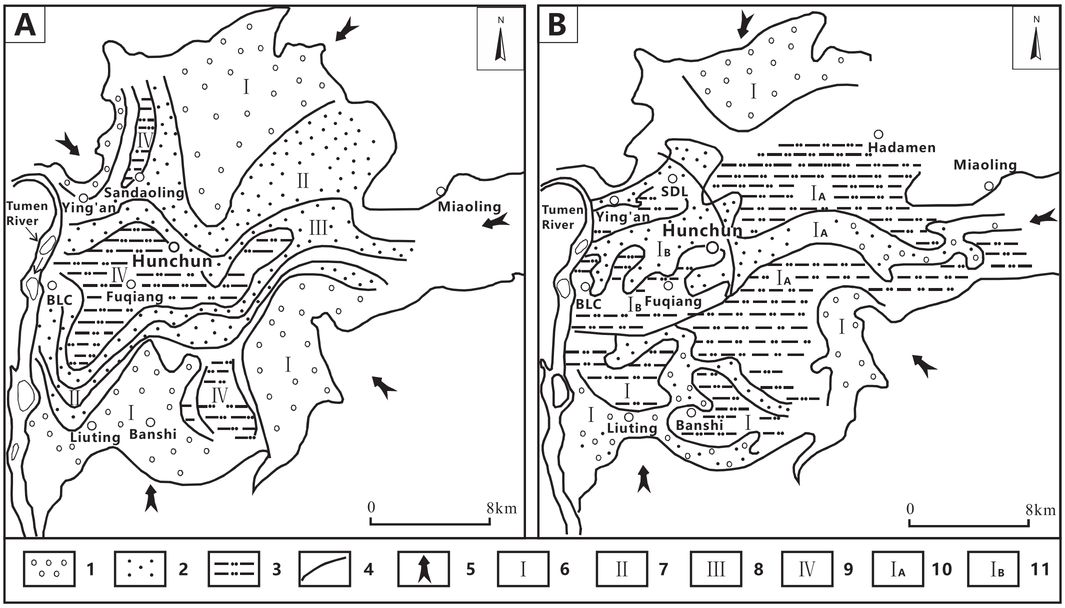


**Fig. 3.** Diagram of sedimentary environment of lower coal-bearing member (A and B, modified from Wang and Wang, 2004). 1. Conglomerate; 2. Sandstone; 3. Siltstone and mudstone; 4. Environment boundary; 5. Terrigenous direction; 6. Alluvial fan; 7. Transitional environment; 8. Fluvial; 9. Lacustrine, swamp; 10. Channel and floodplain; 11. Delta plain.

**Table 1**
Bench thickness (cm), proximate and ultimate analyses (%), total sulfur (%), gross calorific values (MJ/Kg), random huminite reflectance (%), and aluminosilicate mineral content in LTAs (wt%) of the Nos. 23 and 26 coal bench samples.

| Sample | Thickness | $M_{ad}$ | $A_d$ | $V_{daf}$ | $C_{daf}$ | $H_{daf}$ | $N_{daf}$ | $S_{t,d}$ | $Q_{gr,d}$(MJ/kg) | $R_r$ | LTA | Quartz | Kaolinite | Illite | Chlorite | Plagioclase | K-feldspar |
|---|---|---|---|---|---|---|---|---|---|---|---|---|---|---|---|---|---|
| FQ-23-6c | 14 | 14.38 | 43.58 | 53.29 | 77.84 | 5.87 | 1.45 | 0.14 | 16.61 | 0.38 | 51.51 | 26.7 | 28.1 | 27.9 | 2.3 | 5.8 | 5.3 |
| FQ-23-7c | 10 | 18.73 | 20.04 | 43.96 | 80.01 | 4.86 | 1.36 | 0.20 | 23.20 | 0.43 | 25.78 | 27.2 | 39.5 | 21 | | | |
| FQ-23-10c | 12 | 17.78 | 21.39 | 50.36 | 80.08 | 5.55 | 1.51 | 0.10 | 23.83 | 0.35 | 32.72 | 29.6 | 31.9 | 24.7 | | | |
| FQ-23-11c | 16 | 16.07 | 26.18 | 50.69 | 80.07 | 5.54 | 1.45 | 0.12 | 21.92 | 0.33 | 48.32 | 24.6 | 46.5 | 21.3 | | | |
| FQ-23-12c | 15 | 14.81 | 39.64 | 51.40 | 78.54 | 5.56 | 1.55 | 0.14 | 17.72 | 0.31 | 52.80 | 27.5 | 38.6 | 24.6 | | | |
| FQ-23-14c | 17 | 15.85 | 47.07 | 46.45 | 77.46 | 4.85 | 1.29 | 0.12 | 14.41 | 0.36 | 24.63 | 23.5 | 40.7 | 31.6 | | 2.2 | |
| FQ-23-17c | 12 | 17.86 | 28.26 | 50.05 | 80.41 | 5.29 | 1.65 | 0.17 | 20.92 | 0.35 | 35.97 | 26 | 40.3 | 26.1 | | | |
| FQ-23-18c | 15 | 17.64 | 20.86 | 49.26 | 81.08 | 5.36 | 1.46 | 0.16 | 23.47 | 0.34 | 24.64 | 21.4 | 51.7 | 15 | | | |
| FQ-23-19c | 14 | 17.18 | 41.63 | 55.95 | 83.84 | 4.54 | 1.42 | 0.07 | 18.03 | 0.34 | 45.40 | 30.5 | 38.9 | 22.7 | 3 | 2.9 | |
| **WA-FQ-23** | **125*** | **16.56** | **32.93** | **50.27** | **79.85** | **5.27** | **1.46** | **0.13** | **19.74** | **0.35** | **38.34** | **26.1** | **39.9** | **24.0** | **0.59** | **1.27** | **0.59** |
| FQ-26-2c | 20 | 12.05 | 46.84 | 51.09 | 74.91 | 5.35 | 1.37 | 0.12 | 16.19 | 0.48 | 61.18 | 24.1 | 45.4 | 23.3 | | 6.2 | 1.0 |
| FQ-26-5c | 18 | 12.39 | 43.07 | 51.91 | 76.59 | 5.56 | 1.55 | 0.17 | 18.18 | 0.46 | 56.54 | 26.3 | 35.3 | 30.3 | 6.1 | 1.5 | |
| FQ-26-6c | 10 | 15.64 | 18.56 | 47.96 | 80.48 | 5.49 | 1.38 | 0.22 | 27.13 | 0.44 | 26.89 | 23.1 | 51.8 | 23.8 | | | |
| FQ-26-7c | 10 | 13.00 | 43.62 | 50.57 | 73.89 | 5.49 | 1.22 | 0.11 | 16.42 | 0.45 | 52.61 | 6.1 | 83.0 | 10.7 | | | |
| FQ-26-8c | 20 | 16.48 | 19.23 | 46.59 | 81.51 | 5.38 | 1.45 | 0.17 | 26.99 | 0.49 | 22.40 | 24.0 | 52.9 | 21.7 | | | |
| **WA-FQ-26** | **78*** | **13.85** | **34.85** | **49.89** | **77.57** | **5.44** | **1.41** | **0.16** | **20.85** | **0.47** | **44.67** | **22.2** | **50.6** | **23.0** | **1.41** | **1.94** | **0.26** |

M, moisture; A, ash yield; V, volatile matter; C, carbon; H, hydrogen; N, nitrogen; $S_t$, total sulfur; $Q_{gr}$, gross calorific value; ad, as-received basis; d, dry basis; daf, dry and ash-free basis; Rr, random reflectance of huminite; WA, weighted average (weighted by thickness of sample interval); LTA, low-temperature ash yield. * Total thickness of coal benches (cm). The rows in bold are the weighted averages for each coal seam.

42°43′–42°59′N. The Hunchun Coalfield includes several major mines as shown in Fig. 1C. The Fuqiang underground mine (formerly known as the Chengxi Mine) is located in the northwestern part of the coalfield (Fig. 1C).

The Paleogene Hunchun Formation, which consists of typical continental sediments (Fig. 2) and is the coal-bearing sequence in the coalfield, was divided into three parts (Xu and Han, 1990). However, more recently, Wang and Wang (2004) and Wen (2014) divided the Hunchun Formation into six parts, from bottom to top as follows: $E_h^1$, conglomerate member; $E_h^2$, lower coal-bearing member; $E_h^3$ member characterized by brown color and mainly composed of mudstone, siltstone, and sandstone; $E_h^4$, middle coal-bearing member; $E_h^5$ member containing similar lithological compositions with $E_h^3$ member; and, $E_h^6$, upper coal-bearing member.

The lower coal-bearing member ($E_h^2$) (Fig. 2A), with a thickness of 145 m, is a major coal-bearing unit in the Fuqiang mine. It is composed of dark gray mudstone, siltstone, argillaceous siltstone, coal, and white medium/coarse-grained sandstone. This unit includes a marker interval identified as $K_2$ (tuffite), which is located between the Nos. 21 and 23 coal seams and is used to determine the position of coal seams throughout the basin (Wang and Wang, 2004). In some locations, the $K_2$ layer is the roof of the No. 23 coal seam. The $E_h^2$ member consists of one or a few layers of green or grass-green tuffite.

The lower coal-bearing member ($E_h^2$) in the Fuqiang mine contains ~16 coal seams, of which Nos. 19, 23, 26, 26 L, 30, and 32 are minable and the Nos. 19 L, 20, 21 and 31 are locally minable seams (Fig. 2A). The 1.5–2 m thick No. 23 and 26 coal seams (Fig. 2A, B) are currently being mined at the Fuqiang mine. Its roof and floor strata of the No. 23 seam are composed of siltstone and mudstone, respectively. The No. 26 coal seam (Fig. 2A, B) has a thickness of 1.0–1.5 m, and both its roof and floor horizons consist dominantly of siltstone.

The Upper Paleozoic and Mesozoic volcanic and clastic rocks are widely distributed in and around the coalfield. They form the basement of the coal basin and have an unconformable contact with the overlying

**Table 2**
Percentages of major-element oxides (%), concentrations of trace elements (ppm; Hg in ppb), and loss on ignition (LOI, %) for the coals from the Fuqiang mine (on a whole coal basis).

| Sample | LOI | $SiO_2$ | $TiO_2$ | $Al_2O_3$ | $Fe_2O_3$ | MnO | MgO | CaO | $Na_2O$ | $K_2O$ | $P_2O_5$ | Li | Be | B | F | Sc | V | Cr | Co | Ni | Cu | Zn | Ga |
|---|---|---|---|---|---|---|---|---|---|---|---|---|---|---|---|---|---|---|---|---|---|---|---|
| FQ-23-R | 21.55 | 49.36 | 0.62 | 18.27 | 4.64 | 0.030 | 1.08 | 1.12 | 0.84 | 2.46 | 0.028 | 28.7 | 3.05 | 42.3 | 468 | 7.61 | 58.4 | 38.8 | 7.9 | 18.7 | 25.6 | 77.9 | 20.4 |
| FQ-23-1p | 29.06 | 44.89 | 0.57 | 15.72 | 4.42 | 0.028 | 0.92 | 0.98 | 0.83 | 2.57 | 0.016 | 35.9 | 4.46 | 51.8 | 398 | 11.2 | 73.1 | 42.6 | 8.1 | 17.9 | 40.4 | 72.8 | 20.8 |
| FQ-23-2p | 10.04 | 58.34 | 0.82 | 18.06 | 5.80 | 0.052 | 1.53 | 0.69 | 1.20 | 3.44 | 0.039 | 33.0 | 1.80 | 49.3 | 442 | 14.9 | 97.7 | 55.3 | 9.1 | 20.1 | 41.7 | 116 | 21.1 |
| FQ-23-3p | 13.79 | 54.81 | 0.89 | 18.56 | 5.26 | 0.043 | 1.26 | 0.75 | 0.97 | 3.61 | 0.060 | 31.4 | 1.99 | 42.6 | 429 | 9.36 | 98.5 | 56.9 | 8.0 | 19.4 | 36.7 | 119 | 20.5 |
| FQ-23-4p | 16.64 | 53.17 | 0.78 | 17.12 | 5.18 | 0.042 | 1.27 | 0.82 | 0.97 | 3.88 | 0.122 | 31.4 | 2.11 | 44.6 | 505 | 11.7 | 93.1 | 51.3 | 7.8 | 19.6 | 36.0 | 118 | 20.1 |
| FQ-23-5p | 55.42 | 29.19 | 0.44 | 9.71 | 1.67 | 0.017 | 0.43 | 0.83 | 0.51 | 1.77 | 0.012 | 23.6 | 3.85 | 73.4 | 190 | 9.19 | 75.7 | 33.4 | 6.4 | 10.4 | 40.8 | 22.9 | 14.4 |
| FQ-23-6c | 62.69 | 23.11 | 0.37 | 8.76 | 2.01 | 0.022 | 0.48 | 0.93 | 0.38 | 1.23 | 0.011 | 20.0 | 2.89 | 72.2 | 184 | 8.13 | 70.0 | 49.7 | 9.9 | 28.6 | 38.8 | 38.9 | 12.6 |
| FQ-23-7c | 83.72 | 9.64 | 0.18 | 4.25 | 0.73 | 0.012 | 0.10 | 0.88 | 0.17 | 0.33 | 0.006 | 10.5 | 1.32 | 118.4 | 90.8 | 4.73 | 39.5 | 15.4 | 5.2 | 8.7 | 16.7 | 8.1 | 10.1 |
| FQ-23-8p | 31.69 | 41.89 | 0.54 | 18.11 | 3.10 | 0.022 | 0.78 | 0.74 | 0.59 | 2.50 | 0.036 | 64.4 | 1.44 | 62.9 | 383 | 10.8 | 55.8 | 40.9 | 5.4 | 15.6 | 20.5 | 65.4 | 20.8 |
| FQ-23-9p | 42.39 | 35.38 | 0.65 | 15.04 | 2.57 | 0.020 | 0.53 | 0.82 | 0.50 | 2.07 | 0.033 | 58.8 | 1.52 | 71.6 | 310 | 10.7 | 87.8 | 36.7 | 4.7 | 14.4 | 40.1 | 75.3 | 18.2 |
| FQ-23-10c | 82.42 | 10.75 | 0.18 | 4.34 | 0.64 | 0.014 | 0.12 | 0.94 | 0.17 | 0.41 | 0.008 | 11.5 | 1.30 | 93.0 | 107 | 4.62 | 45.2 | 17.0 | 11.1 | 10.9 | 26.2 | 7.3 | 7.3 |
| FQ-23-11c | 78.02 | 13.23 | 0.21 | 6.11 | 0.69 | 0.014 | 0.13 | 0.95 | 0.18 | 0.47 | 0.010 | 15.7 | 1.36 | 91.3 | 116 | 5.42 | 38.3 | 16.7 | 7.9 | 9.7 | 24.7 | 10.0 | 8.8 |
| FQ-23-12c | 66.23 | 21.27 | 0.39 | 9.00 | 0.95 | 0.014 | 0.22 | 0.95 | 0.20 | 0.76 | 0.012 | 21.9 | 1.66 | 81.7 | 195 | 4.75 | 63.9 | 26.6 | 7.5 | 12.3 | 33.6 | 13.1 | 13.9 |
| FQ-23-13p | 38.14 | 37.68 | 0.57 | 17.42 | 2.61 | 0.016 | 0.51 | 0.85 | 0.37 | 1.79 | 0.035 | 75.5 | 1.44 | 67.6 | 372 | 11.5 | 80.7 | 41.4 | 4.8 | 15.6 | 52.8 | 37.9 | 20.3 |
| FQ-23-14c | 60.39 | 23.68 | 0.37 | 10.76 | 1.94 | 0.016 | 0.37 | 0.84 | 0.31 | 1.28 | 0.037 | 33.8 | 1.42 | 88.1 | 258 | 5.88 | 85.8 | 31.4 | 4.5 | 14.4 | 35.3 | 34.6 | 18.4 |
| FQ-23-15p | 39.05 | 37.58 | 0.57 | 15.08 | 3.53 | 0.027 | 0.77 | 0.69 | 0.55 | 2.11 | 0.035 | 56.2 | 1.64 | 61.4 | 325 | 13.0 | 104 | 42.0 | 7.1 | 17.5 | 45.5 | 96.9 | 18.3 |
| FQ-23-16p | 30.63 | 43.30 | 0.64 | 16.83 | 3.99 | 0.028 | 0.80 | 0.75 | 0.62 | 2.37 | 0.043 | 91.0 | 1.56 | 55.6 | 374 | 12.6 | 100 | 44.8 | 6.7 | 20.9 | 46.2 | 92.1 | 19.9 |
| FQ-23-17c | 76.78 | 13.77 | 0.23 | 6.34 | 1.02 | 0.016 | 0.20 | 0.86 | 0.21 | 0.56 | 0.010 | 25.1 | 1.67 | 81.5 | 135 | 7.60 | 72.6 | 25.7 | 17.6 | 17.8 | 41.7 | 16.4 | 9.7 |
| FQ-23-18c | 82.82 | 9.96 | 0.19 | 4.93 | 0.62 | 0.015 | 0.10 | 0.94 | 0.16 | 0.26 | 0.007 | 12.9 | 2.21 | 89.7 | 91.9 | 6.21 | 36.8 | 15.1 | 7.8 | 8.9 | 24.7 | 7.2 | 8.0 |
| FQ-23-19c | 65.52 | 21.44 | 0.37 | 8.79 | 1.46 | 0.017 | 0.30 | 1.00 | 0.32 | 0.76 | 0.020 | 24.4 | 3.93 | 91.5 | 183 | 5.79 | 51.6 | 27.1 | 6.7 | 11.7 | 24.7 | 18.9 | 16.6 |
| FQ-23-F | 10.91 | 54.89 | 0.99 | 21.77 | 5.74 | 0.046 | 1.41 | 0.69 | 0.83 | 2.65 | 0.082 | 42.0 | 1.65 | 35.3 | 458 | 12.1 | 105 | 68.4 | 11.4 | 29.3 | 42.4 | 132 | 22.6 |
| **WA-23** | **72.43** | **16.78** | **0.28** | **7.25** | **1.15** | **0.016** | **0.23** | **0.92** | **0.24** | **0.70** | **0.014** | **20.1** | **1.99** | **88.8** | **156** | **5.92** | **56.7** | **25.3** | **8.5** | **13.7** | **29.9** | **17.8** | **12.0** |
| FQ-26-R | 24.50 | 44.46 | 0.71 | 17.96 | 6.67 | 0.054 | 1.48 | 0.84 | 0.69 | 2.47 | 0.166 | 41.9 | 2.36 | 56.1 | 717 | 16.2 | 138 | 65.7 | 17.9 | 33.3 | 60.0 | 155 | 22.8 |
| FQ-26-1p | 51.48 | 29.96 | 0.47 | 12.32 | 2.46 | 0.022 | 0.55 | 0.78 | 0.45 | 1.49 | 0.014 | 52.7 | 2.03 | 74.2 | 356 | 12.2 | 86.9 | 39.9 | 6.04 | 12.5 | 52.3 | 43.4 | 16.3 |
| FQ-26-2c | 58.81 | 24.88 | 0.39 | 11.34 | 2.05 | 0.018 | 0.39 | 0.85 | 0.33 | 0.92 | 0.016 | 56.3 | 1.51 | 68.9 | 315 | 6.62 | 68.4 | 28.8 | 5.72 | 12.6 | 35.0 | 34.2 | 14.7 |
| FQ-26-3p | 45.67 | 33.76 | 0.55 | 14.31 | 2.56 | 0.019 | 0.49 | 0.86 | 0.39 | 1.37 | 0.017 | 96.1 | 1.64 | 74.6 | 423 | 11.2 | 81.6 | 36.1 | 5.16 | 15.2 | 32.1 | 28.2 | 19.1 |
| FQ-26-4p | 21.79 | 47.76 | 0.68 | 18.46 | 5.98 | 0.047 | 1.34 | 0.64 | 0.57 | 2.70 | 0.038 | 49.2 | 1.49 | 77.6 | 585 | 15.1 | 106 | 56.0 | 7.99 | 21.5 | 45.6 | 134 | 21.4 |
| FQ-26-5c | 62.26 | 22.54 | 0.37 | 10.19 | 1.99 | 0.021 | 0.45 | 0.85 | 0.26 | 1.05 | 0.014 | 33.3 | 1.66 | 75.2 | 295 | 7.97 | 92.7 | 32.3 | 11.9 | 15.8 | 72.0 | 60.2 | 13.6 |
| FQ-26-6c | 84.35 | 8.93 | 0.18 | 4.37 | 0.65 | 0.016 | 0.11 | 0.93 | 0.15 | 0.30 | 0.006 | 10.5 | 1.23 | 102 | 136 | 5.93 | 41.8 | 14.4 | 7.19 | 7.32 | 34.7 | 7.91 | 7.74 |
| FQ-26-7c | 62.05 | 21.00 | 0.31 | 13.66 | 1.47 | 0.018 | 0.21 | 0.77 | 0.16 | 0.33 | 0.029 | 0.53 | 0.97 | 76.5 | 371 | 0.82 | 28.0 | 8.71 | 5.24 | 8.36 | 17.8 | 16.5 | 12.3 |
| FQ-26-8c | 83.94 | 9.42 | 0.18 | 4.23 | 0.67 | 0.016 | 0.11 | 0.99 | 0.16 | 0.26 | 0.006 | 6.80 | 1.27 | 102 | 149 | 4.82 | 31.4 | 12.5 | 7.67 | 6.42 | 25.6 | 4.99 | 6.83 |
| FQ-26-9p | 49.14 | 30.56 | 0.55 | 14.17 | 2.54 | 0.024 | 0.56 | 0.86 | 0.36 | 1.22 | 0.015 | 77.0 | 3.33 | 77.1 | 348 | 13.2 | 102 | 46.3 | 11.1 | 17.3 | 40.0 | 34.9 | 18.9 |
| FQ-26-F | 10.53 | 55.12 | 0.87 | 20.00 | 6.96 | 0.065 | 1.81 | 0.86 | 0.78 | 2.75 | 0.248 | 38.1 | 1.63 | 64.8 | 723 | 16.4 | 122 | 66.8 | 11.8 | 27.2 | 46.9 | 162.9 | 23.9 |
| **WA-26** | **69.74** | **17.84** | **0.30** | **8.66** | **1.43** | **0.018** | **0.27** | **0.89** | **0.23** | **0.63** | **0.013** | **25.3** | **1.38** | **84.1** | **252** | **5.64** | **55.9** | **21.0** | **7.76** | **10.5** | **38.9** | **27.1** | **11.2** |
| Average* | | 8.47 | 0.33 | 5.98 | 4.85 | 0.015 | 0.22 | 1.23 | 0.16 | 0.19 | 0.092 | 10 | 1.2 | 56 | 90 | 4.1 | 22 | 15 | 4.2 | 9 | 15 | 18 | 5.5 |

| Sample | Ge | As | Se | Rb | Sr | Zr | Nb | Mo | Cd | In | Sn | Sb | Cs | Ba | Hf | Ta | W | Hg | Tl | Pb | Bi | Th | U |
|---|---|---|---|---|---|---|---|---|---|---|---|---|---|---|---|---|---|---|---|---|---|---|---|
| FQ-23-R | 1.85 | 17.8 | 0.22 | 34.9 | 191 | 165 | 1.27 | 0.21 | 0.40 | 0.057 | 1.49 | 0.06 | 6.88 | 319 | 4.62 | 0.02 | 0.51 | 62 | 0.41 | 27.7 | 0.60 | 7.85 | 3.76 |
| FQ-23-1p | 6.69 | 6.46 | 0.00 | 61.9 | 209 | 151 | 9.51 | 1.00 | 0.59 | 0.062 | 2.93 | 4.98 | 10.6 | 369 | 4.12 | 0.90 | 5.21 | 175 | 0.57 | 33.4 | 0.83 | 11.9 | 3.35 |
| FQ-23-2p | 1.15 | 10.3 | 0.09 | 91.4 | 162 | 170 | 9.96 | 1.06 | 0.49 | 0.076 | 3.24 | 0.83 | 7.52 | 512 | 4.60 | 0.80 | 7.45 | 42 | 0.55 | 28.3 | 0.66 | 10.7 | 2.85 |
| FQ-23-3p | 1.05 | 10.5 | 0.28 | 41.6 | 118 | 190 | 12.0 | 0.88 | 0.56 | 0.074 | 3.29 | 0.86 | 5.53 | 340 | 5.12 | 0.96 | 8.38 | 47 | 0.46 | 25.1 | 0.61 | 5.68 | 3.19 |
| FQ-23-4p | 1.08 | 8.89 | 0.39 | 79.8 | 150 | 170 | 10.2 | 0.57 | 0.57 | 0.072 | 3.32 | 1.09 | 6.60 | 520 | 4.52 | 0.87 | 6.13 | 106 | 0.57 | 26.8 | 0.63 | 9.16 | 2.79 |
| FQ-23-5p | 3.15 | 3.51 | 0.69 | 54.9 | 142 | 91.0 | 5.63 | 1.97 | 0.37 | 0.048 | 1.95 | 5.49 | 8.15 | 299 | 2.60 | 0.38 | 9.06 | 41 | 0.52 | 23.6 | 0.79 | 6.87 | 2.44 |
| FQ-23-6c | 1.83 | 3.66 | 0.48 | 43.7 | 160 | 81.4 | 4.56 | 5.12 | 0.40 | 0.038 | 1.94 | 2.73 | 7.65 | 242 | 2.24 | 0.44 | 9.55 | 57 | 0.37 | 18.2 | 0.66 | 7.62 | 2.95 |
| FQ-23-7c | 1.77 | 2.40 | 0.45 | 15.8 | 136 | 46.9 | 3.45 | 4.48 | 0.10 | 0.014 | 0.94 | 2.87 | 3.41 | 139 | 1.25 | 0.28 | 18.8 | 10 | 0.47 | 8.46 | 0.35 | 4.42 | 1.53 |
| FQ-23-8p | 1.41 | 3.79 | 0.50 | 84.8 | 150 | 148 | 8.87 | 0.77 | 0.33 | 0.059 | 3.60 | 1.12 | 12.0 | 378 | 4.38 | 1.24 | 6.16 | 68 | 0.60 | 29.0 | 0.50 | 14.4 | 3.20 |
| FQ-23-9p | 1.43 | 3.08 | 0.26 | 60.7 | 155 | 154 | 2.72 | 0.37 | 0.55 | 0.060 | 2.02 | 0.84 | 9.33 | 278 | 4.04 | 0.09 | 4.20 | 88 | 0.63 | 28.6 | 0.65 | 10.1 | 3.36 |
| FQ-23-10c | 0.58 | 2.56 | 0.74 | 25.1 | 131 | 42.7 | 2.21 | 3.34 | 0.15 | 0.016 | 0.88 | 1.82 | 4.74 | 144 | 1.23 | 0.22 | 5.42 | 8 | 0.37 | 12.7 | 0.34 | 5.09 | 1.57 |
| FQ-23-11c | 0.78 | 2.53 | 0.56 | 25.0 | 136 | 60.6 | 4.78 | 3.41 | 0.16 | 0.020 | 1.30 | 1.78 | 4.92 | 153 | 1.75 | 0.69 | 9.73 | 9 | 0.38 | 11.6 | 0.37 | 7.45 | 2.13 |
| FQ-23-12c | 1.23 | 3.06 | 0.07 | 47.6 | 146 | 101 | 6.20 | 1.99 | 0.20 | 0.040 | 1.88 | 2.19 | 11.58 | 194 | 2.77 | 0.61 | 5.19 | 12 | 0.45 | 12.4 | 0.50 | 7.12 | 2.94 |
| FQ-23-13p | 1.71 | 3.01 | 0.16 | 53.2 | 141 | 140 | 7.82 | 0.76 | 0.40 | 0.082 | 3.24 | 1.70 | 20.6 | 207 | 3.90 | 0.70 | 4.28 | 45 | 0.81 | 36.1 | 1.12 | 13.4 | 3.53 |
| FQ-23-14c | 3.37 | 2.36 | 0.19 | 45.0 | 135 | 98.9 | 5.88 | 3.09 | 0.38 | 0.042 | 1.96 | 5.87 | 16.4 | 228 | 2.74 | 0.53 | 10.6 | 22 | 0.62 | 17.4 | 0.57 | 7.93 | 2.68 |

(*continued on next page*)

**Table 2** (*continued*)

| Sample | Ge | As | Se | Rb | Sr | Zr | Nb | Mo | Cd | In | Sn | Sb | Cs | Ba | Hf | Ta | W | Hg | Tl | Pb | Bi | Th | U |
|---|---|---|---|---|---|---|---|---|---|---|---|---|---|---|---|---|---|---|---|---|---|---|---|
| FQ-23-15p | 1.19 | 2.99 | 0.30 | 62.7 | 126 | 142 | 7.33 | 0.98 | 0.51 | 0.066 | 2.69 | 1.72 | 8.42 | 307 | 3.84 | 0.58 | 4.43 | 105 | 0.63 | 25.9 | 0.73 | 11.3 | 2.86 |
| FQ-23-16p | 1.14 | 4.77 | 0.32 | 61.7 | 139 | 157 | 8.16 | 0.68 | 0.59 | 0.078 | 3.16 | 1.15 | 12.0 | 326 | 4.32 | 0.69 | 5.01 | 68 | 0.63 | 38.1 | 0.99 | 12.2 | 3.54 |
| FQ-23-17c | 1.23 | 4.31 | 0.96 | 25.6 | 128 | 57.1 | 3.88 | 2.86 | 0.29 | 0.030 | 1.21 | 3.13 | 5.27 | 156 | 1.62 | 0.35 | 7.43 | 24 | 0.39 | 18.6 | 0.58 | 7.66 | 2.10 |
| FQ-23-18c | 0.84 | 2.50 | 0.50 | 16.2 | 141 | 72.1 | 4.43 | 2.23 | 0.17 | 0.028 | 1.12 | 1.57 | 3.82 | 134 | 1.95 | 0.38 | 13.0 | 12 | 0.38 | 14.2 | 0.56 | 6.95 | 2.17 |
| FQ-23-19c | 3.31 | 3.90 | 0.76 | 31.1 | 143 | 92.7 | 5.17 | 1.01 | 0.18 | 0.038 | 1.61 | 4.53 | 5.88 | 192 | 2.54 | 0.46 | 17.0 | 47 | 0.51 | 16.2 | 0.42 | 6.89 | 2.18 |
| FQ-23-F | 1.24 | 14.6 | 0.07 | 53.6 | 114 | 197 | 12.7 | 0.21 | 0.50 | 0.086 | 3.50 | 0.68 | 6.90 | 336 | 5.52 | 1.15 | 7.77 | 42 | 0.39 | 27.9 | 0.67 | 11.6 | 3.40 |
| **WA-23** | **1.70** | **3.01** | **0.50** | **31.5** | **140** | **74.8** | **4.64** | **3.00** | **0.23** | **0.031** | **1.47** | **2.99** | **7.45** | **178** | **2.07** | **0.46** | **10.6** | **23** | **0.44** | **14.6** | **0.49** | **6.92** | **2.30** |
| FQ-26-R | 1.33 | 10.8 | 0.54 | 79.8 | 123 | 155 | 9.13 | 1.00 | 0.86 | 0.092 | 3.64 | 2.19 | 11.1 | 405 | 4.36 | 0.68 | 5.82 | 64 | 0.61 | 38.7 | 1.12 | 12.5 | 3.45 |
| FQ-26-1p | 1.66 | 3.35 | 0.23 | 70.1 | 129 | 118 | 5.75 | 0.49 | 0.52 | 0.064 | 2.55 | 2.45 | 12.9 | 305 | 3.39 | 0.45 | 7.07 | 108 | 0.75 | 35.6 | 0.90 | 10.3 | 3.04 |
| FQ-26-2c | 1.43 | 4.16 | 0.06 | 44.9 | 116 | 94.3 | 7.94 | 1.37 | 0.31 | 0.048 | 2.42 | 2.47 | 8.8 | 214 | 2.82 | 1.82 | 9.38 | 103 | 0.67 | 23.0 | 0.65 | 9.02 | 3.26 |
| FQ-26-3p | 1.57 | 2.54 | 0.00 | 74.9 | 143 | 136 | 7.50 | 0.49 | 0.33 | 0.066 | 3.02 | 1.97 | 14.2 | 296 | 3.93 | 0.60 | 6.14 | 45 | 0.69 | 28.1 | 0.76 | 9.82 | 3.21 |
| FQ-26-4p | 1.29 | 6.24 | 0.11 | 86.0 | 104 | 136 | 7.29 | 0.20 | 0.53 | 0.087 | 3.52 | 1.39 | 11.7 | 395 | 3.90 | 0.55 | 5.61 | 101 | 0.57 | 32.1 | 1.03 | 11.1 | 3.05 |
| FQ-26-5c | 1.75 | 4.13 | 0.39 | 46.1 | 113 | 85.5 | 4.69 | 2.13 | 0.88 | 0.058 | 2.16 | 4.40 | 9.16 | 210 | 2.45 | 0.62 | 6.38 | 70 | 0.59 | 25.2 | 1.44 | 8.05 | 3.20 |
| FQ-26-6c | 1.30 | 2.73 | 1.04 | 23.8 | 110 | 40.4 | 2.83 | 2.35 | 0.19 | 0.026 | 1.08 | 2.70 | 4.71 | 118 | 1.21 | 0.26 | 7.80 | 23 | 0.52 | 17.8 | 0.68 | 5.56 | 1.98 |
| FQ-26-7c | 1.36 | 3.50 | 0.31 | 13.6 | 79 | 130 | 9.03 | 1.48 | 0.30 | 0.060 | 3.19 | 1.48 | 2.38 | 92.7 | 4.43 | 0.91 | 5.63 | 30 | 0.35 | 25.9 | 0.68 | 3.32 | 3.08 |
| FQ-26-8c | 0.85 | 1.98 | 0.71 | 13.2 | 114 | 43.9 | 2.45 | 2.39 | 0.16 | 0.018 | 0.91 | 1.56 | 4.00 | 113 | 1.30 | 0.23 | 8.09 | 11 | 0.44 | 11.0 | 0.40 | 4.61 | 1.64 |
| FQ-26-9p | 5.43 | 4.82 | 0.00 | 46.7 | 122 | 136 | 7.77 | 1.05 | 0.34 | 0.056 | 2.60 | 7.41 | 9.63 | 253 | 3.75 | 0.57 | 5.60 | 89 | 0.50 | 25.2 | 0.55 | 9.99 | 2.89 |
| FQ-26-F | 1.34 | 10.9 | 0.41 | 76.9 | 103 | 183 | 9.60 | 0.97 | 0.63 | 0.092 | 3.73 | 0.94 | 7.59 | 434 | 5.12 | 0.75 | 7.63 | 50 | 0.44 | 31.0 | 0.65 | 9.90 | 3.15 |
| **WA-26** | **1.33** | **3.33** | **0.46** | **30.3** | **109** | **77.0** | **5.27** | **1.95** | **0.39** | **0.041** | **1.90** | **2.59** | **6.30** | **159** | **2.34** | **0.82** | **7.67** | **52** | **0.53** | **20.1** | **0.78** | **6.49** | **2.64** |
| Average* | 2 | 7.6 | 1 | 10 | 120 | 35 | 3.3 | 2.2 | 0.24 | 0.02 | 0.79 | 0.84 | 0.98 | 150 | 1.2 | 0.26 | 1.2 | 100 | 0.68 | 6.6 | 0.84 | 3.3 | 2.6 |

* Average content of major-element oxides for common Chinese coals are from Dai et al. (2012b); average concentrations of trace elements are from Ketris and Yudovich (2009). WA, weighted average (weighted by thickness of sample interval). The rows in bold are the weighted averages for each coal seam.


**Fig. 4.** Concentration coefficients (CC) of trace elements in the Fuqiang coals and partings, normalized by average trace element concentrations in the world low-rank coals (Ketris and Yudovich, 2009) and world clays Grigoriev (2009) respectively.

coal-bearing Hunchun Formation. Faults trending NNE, NEE and W-E are well developed within the coal basin (Fig. 1C).

According to Wang and Wang (2004), there were two different sedimentary environments in the Hunchun Basin in the lower coal-bearing member ($E_h^2$), based on the characteristics of lithological compositions of the sediments. Coal seams from Nos. 30 to 23 were formed in alluvial fan, fluvial, and lacustrine environments in stage I (Fig. 3A), and coal seams above No. 23 (from Nos. 21 lower to 19) were deposited in alluvial fan, fluvial, and delta plain environments in stage II (Fig. 3B). The basin was relatively low in the middle and western parts, but the surrounding areas to the north, east and south of the basin are high during deposition of the coal-bearing sequences and thus these areas could have provided terrigenous materials for the sediments in the basin (Fig. 3).

## 3. Samples and methods

### 3.1. Sample collection

A total of 32 bench samples (including 14 coal benches and 18 non-

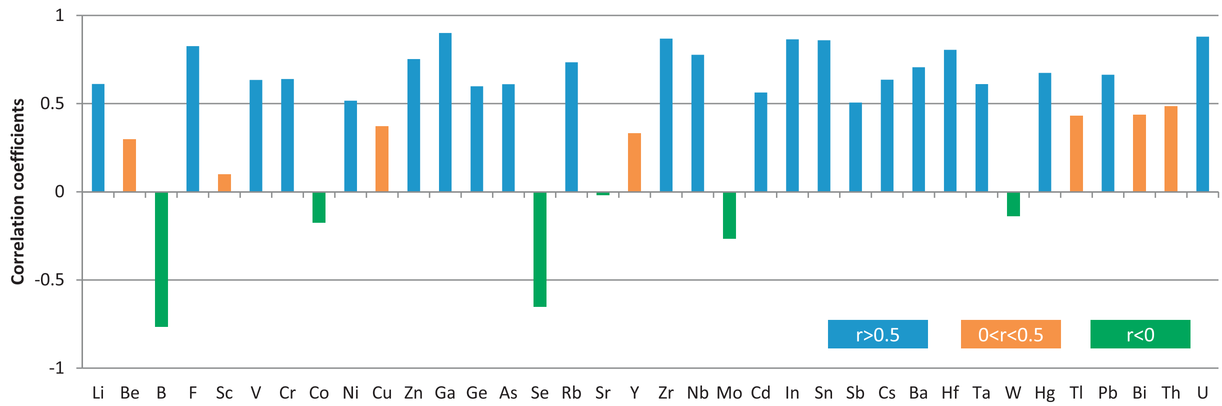


**Fig. 5.** Correlation coefficients (r) between ash yield and trace elements.

coal roof, parting and floor strata) of the Nos. 23 and 26 coals were collected from the underground working faces at the Fuqiang mine of the Hunchun Coalfield. From top to bottom, the samples (except the roof and floor ones) are numbered in an increasing order as indicated in Fig. 2B. The cumulative thickness of the Nos. 23 and 26 coals are respectively 2.85 m and 1.60 m, including partings, which account for 56.1% and 51.3% of the total thickness of the seams, respectively.

### 3.2. Analytical methods

The proximate analysis including the determination of moisture, ash yield, volatile matter, and total sulfur, as well as gross calorific values, were conducted according to ASTM Standards D3174-12 (2012), D3173M-17a (2017), D3175-17 (2017), D3177-02 (2011), and D5865-13 (2013), respectively. A Vario Macro Elemental Analyzer was used to determine the C, H, and N contents in the coal bench samples. Mean random reflectance values of huminite were measured using a Leica DM-4500P microscope equipped with a Craic QDI 302™ spectrophotometer based on ASTM Standard D2798-11a (2011).

The concentrations of trace elements (except F and Hg) in the samples were determined by inductively coupled plasma mass spectrometry (ICP-MS) following the methods described in detail by Dai et al. (2014a) and Li et al. (2014). X-ray fluorescence spectrometry (XRF) was used to determine the concentrations of major-element oxides ($SiO_2$, $TiO_2$, $Al_2O_3$, $Fe_2O_3$, MgO, CaO, MnO, $Na_2O$, $K_2O$, and $P_2O_5$) for each sample after ashing at 815 °C. A Milestone DMA-80 Hg analyzer was used to determine the Hg concentration in all samples. The concentration of fluorine in each sample was determined by pyrohydrolysis, with an ion-selective electrode, according to ASTM Standard D5987-96 (2015).

Aliquots of all the coal bench samples were subjected to low temperature ashing (LTA, < 150 °C), and subsequent determination of mineral phases by X-ray powder diffraction (XRD). Quantitative analysis of minerals was conducted using the Siroquant technique, described in detail by Ward et al. (2001) and Liu et al. (2018).

## 4. Results

### 4.1. Coal chemistry and huminite reflectance

Table 1 displays the proximate analyses (moisture content, ash yield, and volatile matter content) and ultimate analyses (content of C, H, N), total-S content, gross calorific values, random huminite reflectance values, and aluminosilicate mineral compositions in LTAs of all samples of the Nos. 23 and 26 coal benches. The two coals are classified as a medium-high ash coal according to the ash-yield-based Chinese standard classification (GB/T 15224.1-2010, 2010; coals with ash yields 30.01–40.0% are classified as medium-high ash coal). The Nos. 23 and 26 coals have very low total S content (0.13% and 0.16% on average, respectively) and are, therefore, classified as low-sulfur coals, based on the classification by Chou (2012). The two coals have high moisture contents (average values of 16.56% and 13.85%, respectively).

The volatile matter yields, gross calorific values, and random huminite reflectance values (Table 1) indicate a lignite-subbituminous coal rank based on the ASTM classification D388-12 (2012). The huminite reflectance increases from the No. 23 seam (0.35%) to the No. 26 seam (0.47%). It is noteworthy that these characteristics of the low rank and low calorific values for the Fuqiang coals are similar to those in the three coal-hosted Ge deposits that are currently being mined at the Wulantuga, Lincang (both in China), and Spetzugli (Far Eastern Russia) (Dai et al., 2012a, 2015a; Medvedev et al., 1997). The Spetzugli Ge deposit is located in a few hundred kilometers to NE of the study area.

### 4.2. Geochemistry

#### 4.2.1. Abundances of major oxides and trace elements

Table 2 presents the percentages of major-element oxides (wt%) and concentrations of trace elements (ppm) in the Nos. 23 and 26 coals (on a whole coal basis), as well as their comparisons with the average values for Chinese coals (Dai et al., 2012b) and world low-rank coals (Ketris and Yudovich, 2009).

The percentages of major-element oxides in the Fuqiang coals are generally similar to the average values for Chinese coals (Table 2; Dai et al., 2012b). However, percentages of $K_2O$ and $SiO_2$ are higher and $Na_2O$ and $Al_2O_3$ are slightly higher in the Fuqiang coals, probably due to the relatively high amounts of illite and feldspar (plagioclase and K-feldspar). Percentages of $TiO_2$, MgO, CaO, and MnO are either lower than or close to the average values for Chinese coals, while those of $Fe_2O_3$ and $P_2O_5$ are distinctly lower.

Coal bench sample FQ-26-7c, has the lowest $SiO_2/Al_2O_3$ ratio value (1.54), whilst this ratio in other coal bench samples are > 2 (2.30 and 2.10 on average for Nos. 23 and 26 coals, respectively). These are much higher than that of the average value for Chinese coals (1.42; Dai et al., 2012b) and the theoretical value for kaolinite (1.18). The higher $SiO_2/Al_2O_3$ values in these coals are probably due to the high content of quartz and the occurrence of feldspar. The lowest $SiO_2/Al_2O_3$ value of sample FQ-26-7c is due to the lower proportion of quartz (Table 1).

The two coals present similar trace-element abundances (Table 2; Fig. 4). Compared with averages for the common world low-rank coals by Ketris and Yudovich (2009), W and Cs are enriched in the Fuqiang coals ($5 < CC < 10$) (CC, the ratio of an element concentration in the Fuqiang coals vs. the corresponding average value in the world common low-rank coals). The elements Li, V, Ga, Rb, Zr, Sb, and Pb are slightly enriched in the two coals. In addition, F, Cu, Sn and Ta are slightly enriched in the No. 26 seam ($2 < CC < 5$). The two coals are

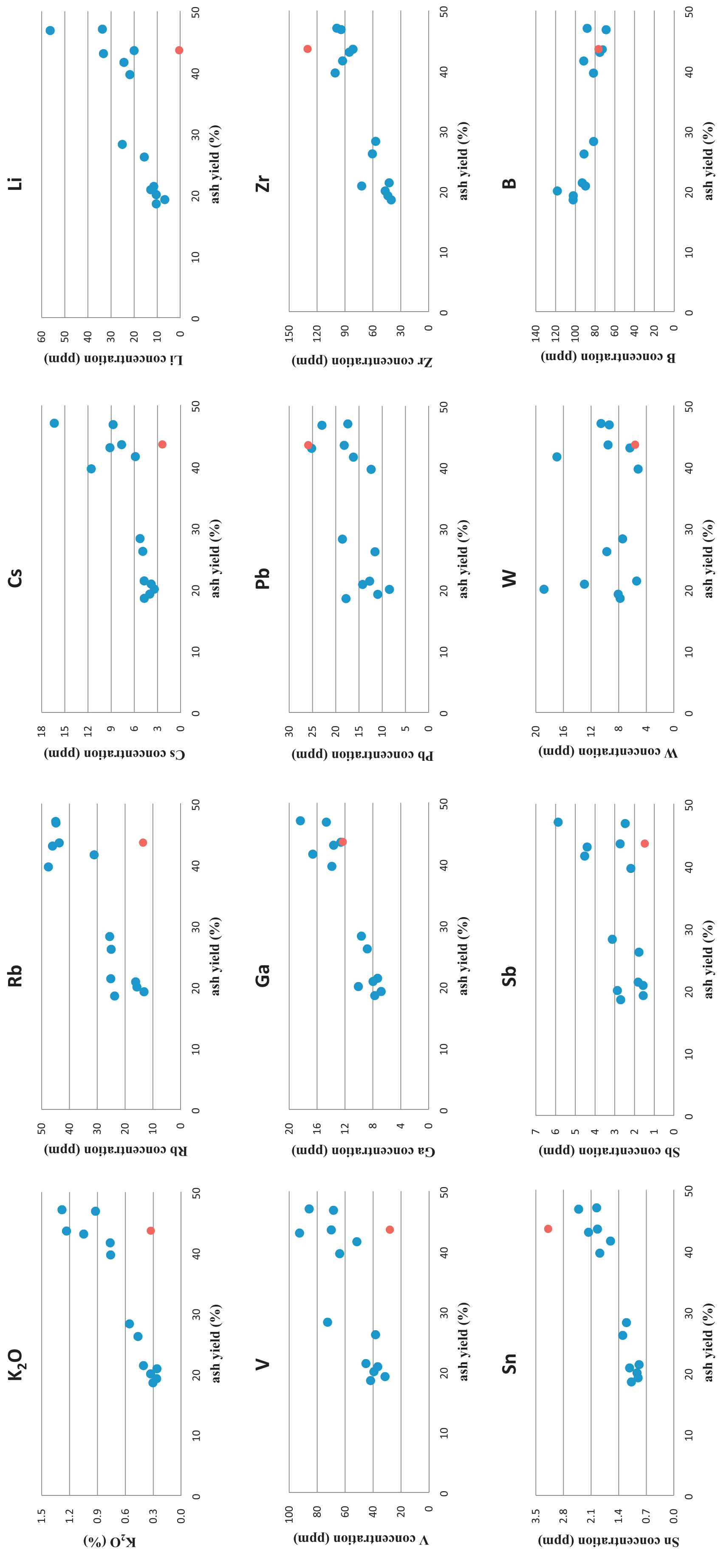


**Fig. 6.** Relation between ash yield and concentrations of selected elements in samples.

**Table 3**
Correlation coefficients between ash yield and selected elements, between selected trace elements and major elements, and between selected trace elements and ash yield of the Fuqiang coals.

| | | | | |
|---|---|---|---|---|
| Li-ash = 0.61 | Rb-ash = 0.73 | Cs-ash = 0.64 | Ga-ash = 0.90 | Zr-ash = 0.87 |
| V-ash = 0.63 | Pb-ash = 0.66 | Sb-ash = 0.51 | W-ash = −0.14 | |
| Li-$Al_2O_3$ = 0.45 | Li-$SiO_2$ = 0.65 | Li-$K_2O$ = 0.71 | Li-$Na_20$ = 0.71 | |
| Rb-$Al_2O_3$ = 0.52 | Rb-$SiO_2$ = 0.78 | Rb-$K_2O$ = 0.90 | Rb-$Na_20$ = 0.75 | |
| Cs-$Al_2O_3$ = 0.46 | Cs-$SiO_2$ = 0.66 | Cs-$K_2O$ = 0.80 | Cs-$Na_20$ = 0.58 | Cs-Rb = 0.85 |
| Ga-$Al_2O_3$ = 0.79 | Ga-$SiO_2$ = 0.89 | Ga-$K_2O$ = 0.80 | Ga-$Na_20$ = 0.75 | |
| Zr-$Al_2O_3$ = 0.94 | Zr-$SiO_2$ = 0.84 | Zr-$K_2O$ = 0.48 | Zr-$Na_20$ = 0.43 | |
| V-$Al_2O_3$ = 0.43 | V-$SiO_2$ = 0.66 | V-$K_2O$ = 0.87 | V-$Na_20$ = 0.69 | |
| Pb-$S_{t,d}$ = −0.07 | Sb- $S_{t,d}$ = −0.06 | Pb-Zn = 0.68 | Sb-Zn = 0.60 | |

depleted in As, Se and Hg (CC < 0.5) and have similar concentrations (0.5 < CC < 2) of the remaining elements to the averages for the world low-rank coals (Table 2; Fig. 4).

Compared with the average values for world clays (Grigoriev, 2009), the partings of No. 23 coal are only slightly enriched in W, Pb, and Bi (CC = 1.88); and the partings in No. 26 coal are enriched in W (5 < CC < 10) and slightly enriched in Sb, Pb, and Bi. The remaining elements are either depleted or close to the average values for world clays (Table 2; Fig. 4).

The roof and floor of the Nos. 23 and 26 coal seams show similar enrichment patterns and are similar to those of the partings, in comparison with the worldwide clays (Grigoriev (2009). With the exception of sample FQ-23-F, which is depleted in W, other non-coal rocks are all slightly enriched in W, Pb and Bi.

#### *4.2.2. Modes of occurrence of some elements in the coals*

Concentrations of most trace elements in the Fuqiang coals are positively correlated with ash-yield (correlation coefficient r > 0.5; Figs. 4, 5), indicating an inorganic affinity. However for some trace elements, correlation coefficients values are low (Be, Sc, Cu, Y, Tl, and Bi) or negative (B, Co, Se, Mo, and W) indicating organic affinity or both organic/inorganic affinities. (Fig. 6.)

According to the correlation coefficients between their concentrations and ash yields, the elements with distinctly elevated concentrations in the Fuqiang coals can be classified into three groups:

1) Group 1 including F, Ga, Zr, and Sn, with relatively high correlation coefficients (r > 0.75), indicating a high inorganic affinity. Gallium and Zr are more positively correlated to $SiO_2$ and $Al_2O_3$ than to $K_2O$ and $Na_2O$ (Table 3), indicating that Ga and Zr in the coals occur mainly in kaolinite.
2) Group 2 consisting of Li, V, Cu, Rb, Sb, Cs, Ta, Pb and Th, with correlation coefficients with ash yields ranging from 0.36 to 0.75, indicating a moderate inorganic affinity.

Positive correlations have been observed between Li and $K_2O$ (r = 0.71), Li and $Na_2O$ (r = 0.71), Li and $SiO_2$ (r = 0.65), and Li and $Al_2O_3$ (r = 0.45), indicating that clay minerals are the major carriers for Li in the coals. Vanadium, like Li, is highly correlated to $K_2O$, indicating that V mainly occurs in K-bearing minerals.

There are also strong correlations between Rb and Cs (r = 0.85), as well as Rb-ash (r = 0.73), Rb-$K_2O$ (r = 0.90), Rb-$SiO_2$ (r = 0.78), Cs-ash (r = 0.64), Cs-$K_2O$ (r = 0.83) and Cs-$SiO_2$ (r = 0.66), but low correlation coefficients between Rb-$Al_2O_3$ (r = 0.52) and Cs-$Al_2O_3$ (r = 0.46). However, correlation coefficients of Li-$Al_2O_3$, Rb-$Al_2O_3$, and Cs-$Al_2O_3$ are high (r = 0.88, 0.92, 0.81, respectively) if sample FQ-26-7c is excluded in this calculation. Sample FQ-26-7c has unusual mineralogical and geochemical features (described more fully below). Therefore, K-bearing clay minerals (e.g., illite) are major carriers of Rb and Cs in the Fuqiang coals.

Antimony and Pb in coal are generally associated with sulfide minerals (e.g., Finkelman et al., 2017; Qin et al., 2018; Dai et al., 2015a). In this study, concentrations of Sb and Pb are weakly correlated with total sulfur (r = −0.06 and r = −0.07, respectively), while sulfides are all below the detection limit of the XRD technique. However, correlation coefficients for Pb—Zn and Sb—Zn are 0.68 and 0.60, respectively, indicating that Pb and Sb may be associated with some Zn-bearing minerals.

3) Only W is weakly correlated to ash yield (r = −0.14), indicating an organic-inorganic mixed affinity. Tungsten is the most enriched element in the Fuqiang coals and has a unique behavior as indicated by its highest W content (18.8 ppm) in the lowest-ash-yield (~20%) coal bench sample FQ-23-7c, showing a sharp contrast with other enriched elements (e.g., Li, V, Ga, Zr, Rb and Cs) (Fig. 7). In addition, the W enrichment in these sections correlates with a distinct depletion in Ge relative to the world low-rank coals (Fig. 4; Ketris and Yudovich, 2009). This differs from the behaviour of Ge—W enrichment assemblage in the large coal-hosted Wulantuga, Lincang, Spetzugli coal deposits (Dai et al., 2012a, 2015a; Seredin et al., 2006), as well as from Ge—W relations in the low-Ge coal of the Shengli Coalfield (Dai et al., 2015b) and the BLC 19–2 coal in the Hunchun basin (Dai et al., 2018).

#### *4.2.3. Distribution patterns of REY in coal and host rocks*

For many years rare earth elements and yttrium (REY) have been widely used as geochemical indicators of the sediment-source area, sedimentary condition, and post-depositional history of coal deposits (Qi et al., 2007; Seredin and Finkelman, 2008; Seredin and Dai, 2012; Hower et al., 2015a; Dai et al., 2015c, 2016b). In the present study, the concentrations of REY are normalized to UCC (upper continental crust; Taylor and McLennan, 1985) in order to identify characteristics of REY distribution patterns in the samples investigated. The geochemical classification by Seredin and Dai (2012) distinguishes three types of REY enrichment: L-type ($La_N/Lu_N$ > 1), M-type ($La_N/Sm_N$ < 1, $Gd_N/Lu_N$ > 1), and H-type ($La_N/Lu_N$ < 1; where $_N$ stands for the normalization of REY concentration in samples to UCC).

Based on Dai et al. (2016b), anomalies of Ce, Eu, and Gd ($Ce_N/Ce_N^*$, $Eu_N/Eu_N^*$ and $Gd_N/Gd_N^*$, respectively) in coal and sedimentary rocks are calculated using the following formulae (where * stands for the theoretical normalized values of REY, calculated from its two neighboring elements in the periodic table):

$$Ce_N/Ce_N^* = Ce_N/(0.5La_N + 0.5Pr_N) \quad (1)$$

$$Eu_N/Eu_N^* = Eu_N/[(Sm_N \times 0.67) + (Tb_N \times 0.33)] \quad (2)$$

$$Gd_N/Gd_N^* = Gd_N/[(Sm_N \times 0.33) + (Tb_N \times 0.67)] \quad (3)$$

The total concentrations of REY in the Nos. 23 and 26 Coals are 95.1 and 87.1 μg/g, respectively (Table 4), slightly higher than the average value for the average world lignites and subbituminous coals (65.3 μg/g; Ketris and Yudovich, 2009). The REY in the Fuqiang samples, including coal plies, partings and host rocks are mainly represented by the M- and H-REY joint enrichment, and, to a lesser extent, H-REY enrichment types (Fig. 8), except for sample FQ-26-7c with a L- and M-REY joint enrichment type.

Coal samples from the No. 23 seam have distinct positive Gd

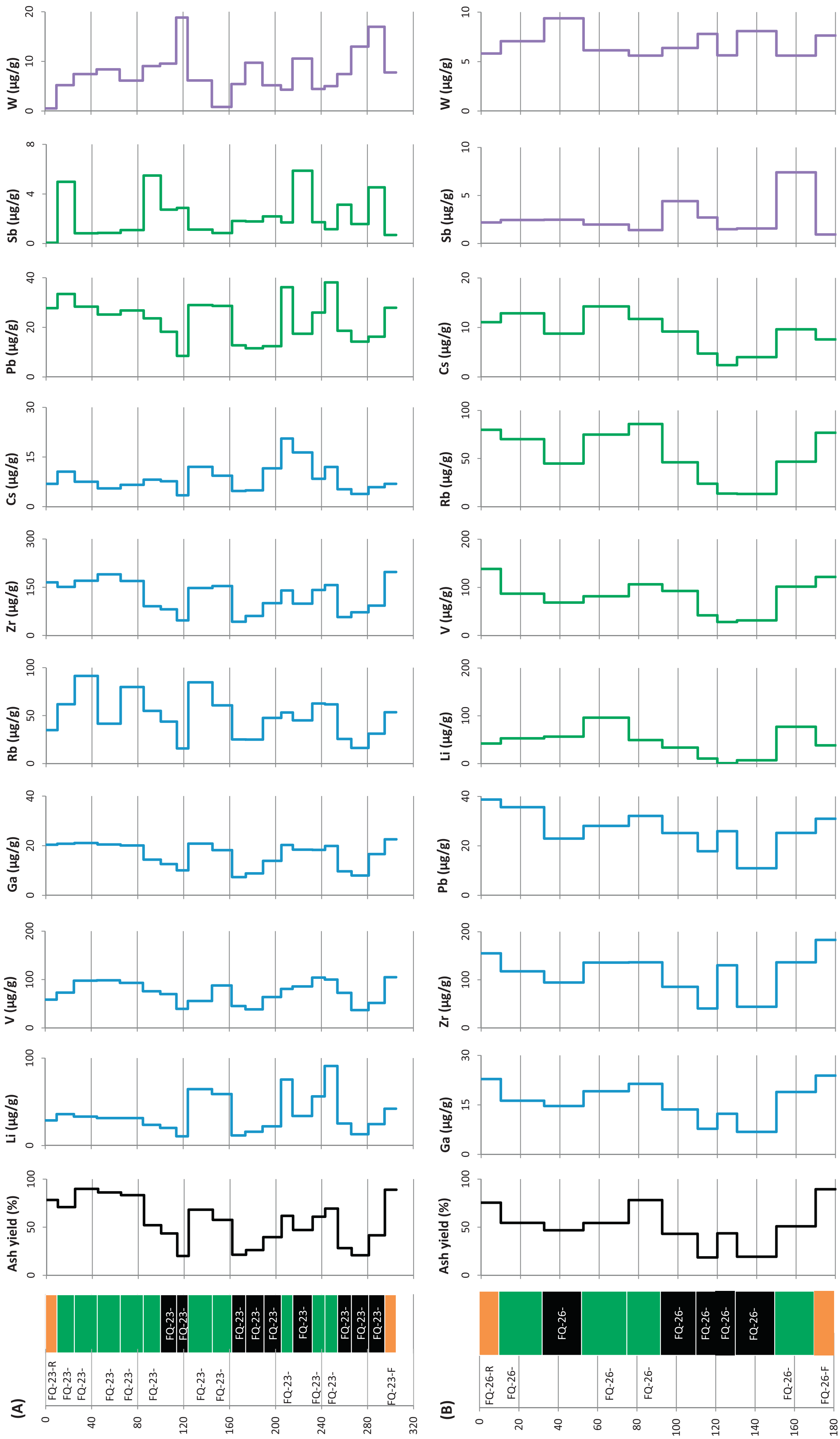


**Fig. 7**. Variations in concentration of selected rock components through the studied coal sections.

**Table 4**
Concentrations of rare earth elements and Y in the Nos. 23 and 26 coals from the Fuqiang mine.

| Sample | La | Ce | Pr | Nd | Sm | Eu | Gd | Tb | Dy | Y | Ho | Er | Tm | Yb | Lu | REY | $Eu_N/Eu_N^*$ | $Gd_N/Gd_N^*$ | Type |
|---|---|---|---|---|---|---|---|---|---|---|---|---|---|---|---|---|---|---|---|
| FQ-23-R | 15.3 | 40.7 | 3.59 | 13.3 | 2.59 | 0.55 | 2.69 | 0.41 | 2.35 | 9.11 | 0.51 | 1.52 | 0.24 | 1.60 | 0.25 | 94.71 | 1.04 | 1.18 | H |
| FQ-23-1p | 24.9 | 52.6 | 5.49 | 21.0 | 4.13 | 0.90 | 4.25 | 0.63 | 3.86 | 19.9 | 0.79 | 2.45 | 0.35 | 2.34 | 0.36 | 143.93 | 1.09 | 1.19 | H |
| FQ-23-2p | 30.7 | 65.8 | 6.83 | 27.0 | 5.50 | 1.21 | 5.64 | 0.78 | 4.52 | 22.0 | 0.86 | 2.65 | 0.39 | 2.66 | 0.40 | 176.85 | 1.13 | 1.21 | M-H |
| FQ-23-3p | 15.7 | 52.1 | 4.23 | 17.1 | 3.51 | 0.84 | 3.79 | 0.54 | 3.27 | 12.0 | 0.65 | 1.95 | 0.28 | 1.95 | 0.30 | 118.18 | 1.19 | 1.25 | M-H |
| FQ-23-4p | 26.0 | 61.0 | 6.08 | 24.2 | 4.80 | 1.11 | 5.12 | 0.68 | 4.04 | 19.5 | 0.78 | 2.30 | 0.32 | 2.19 | 0.32 | 158.48 | 1.18 | 1.26 | M-H |
| FQ-23-5p | 18.5 | 39.6 | 4.27 | 17.4 | 3.60 | 0.85 | 4.09 | 0.60 | 3.50 | 19.8 | 0.70 | 2.14 | 0.30 | 2.08 | 0.30 | 117.73 | 1.14 | 1.28 | M-H |
| FQ-23-6c | 19.7 | 42.0 | 4.63 | 18.5 | 3.81 | 0.89 | 4.09 | 0.60 | 3.51 | 18.4 | 0.68 | 2.02 | 0.27 | 1.92 | 0.27 | 121.31 | 1.15 | 1.23 | M-H |
| FQ-23-7c | 8.45 | 17.1 | 1.91 | 7.64 | 1.63 | 0.39 | 1.95 | 0.30 | 1.80 | 10.2 | 0.37 | 1.09 | 0.15 | 1.07 | 0.15 | 54.22 | 1.13 | 1.29 | M-H |
| FQ-23-8p | 27.0 | 55.7 | 5.81 | 22.5 | 4.54 | 0.89 | 4.63 | 0.63 | 3.67 | 18.4 | 0.70 | 2.18 | 0.31 | 2.20 | 0.33 | 149.37 | 1.01 | 1.22 | M-H |
| FQ-23-9p | 26.6 | 60.2 | 6.05 | 23.7 | 4.63 | 1.00 | 4.75 | 0.67 | 3.78 | 17.5 | 0.72 | 2.15 | 0.30 | 2.10 | 0.31 | 154.55 | 1.10 | 1.21 | M-H |
| FQ-23-10c | 12.4 | 30.3 | 2.71 | 10.3 | 2.01 | 0.44 | 2.21 | 0.31 | 1.78 | 9.93 | 0.35 | 1.03 | 0.15 | 1.01 | 0.15 | 75.06 | 1.09 | 1.28 | M-H |
| FQ-23-11c | 14.1 | 33.2 | 3.21 | 12.5 | 2.55 | 0.52 | 2.74 | 0.38 | 2.28 | 11.6 | 0.44 | 1.31 | 0.19 | 1.31 | 0.19 | 86.52 | 1.03 | 1.25 | M-H |
| FQ-23-12c | 16.2 | 33.6 | 3.44 | 13.2 | 2.64 | 0.56 | 2.92 | 0.40 | 2.34 | 12.7 | 0.47 | 1.42 | 0.19 | 1.37 | 0.22 | 91.66 | 1.06 | 1.28 | M-H |
| FQ-23-13p | 21.0 | 52.7 | 5.24 | 21.1 | 4.52 | 0.93 | 4.69 | 0.68 | 4.02 | 19.3 | 0.78 | 2.37 | 0.34 | 2.37 | 0.35 | 140.48 | 1.03 | 1.21 | M-H |
| FQ-23-14c | 17.4 | 35.6 | 3.94 | 15.7 | 3.35 | 0.74 | 3.75 | 0.56 | 3.39 | 17.4 | 0.67 | 2.00 | 0.28 | 1.91 | 0.29 | 106.98 | 1.07 | 1.25 | M-H |
| FQ-23-15p | 31.0 | 69.4 | 7.03 | 27.7 | 5.40 | 1.17 | 5.55 | 0.76 | 4.35 | 21.0 | 0.82 | 2.45 | 0.35 | 2.39 | 0.34 | 179.69 | 1.11 | 1.22 | M-H |
| FQ-23-16p | 31.3 | 72.4 | 7.27 | 28.5 | 5.81 | 1.20 | 5.98 | 0.83 | 4.68 | 23.0 | 0.90 | 2.66 | 0.37 | 2.61 | 0.38 | 187.90 | 1.05 | 1.22 | M-H |
| FQ-23-17c | 19.8 | 47.9 | 4.79 | 19.3 | 3.95 | 0.87 | 4.30 | 0.60 | 3.55 | 17.5 | 0.67 | 1.97 | 0.27 | 1.81 | 0.27 | 127.55 | 1.10 | 1.26 | M-H |
| FQ-23-18c | 12.5 | 28.8 | 2.95 | 12.0 | 2.53 | 0.55 | 2.82 | 0.41 | 2.57 | 12.9 | 0.50 | 1.54 | 0.22 | 1.49 | 0.23 | 82.03 | 1.07 | 1.26 | M-H |
| FQ-23-19c | 14.0 | 30.1 | 3.30 | 13.4 | 2.78 | 0.68 | 3.49 | 0.55 | 3.64 | 23.2 | 0.76 | 2.29 | 0.31 | 2.13 | 0.33 | 100.91 | 1.11 | 1.32 | H |
| FQ-23-F | 30.4 | 69.9 | 6.89 | 27.3 | 5.55 | 1.22 | 5.89 | 0.82 | 4.71 | 23.8 | 0.92 | 2.78 | 0.41 | 2.77 | 0.41 | 183.71 | 1.11 | 1.24 | M-H |
| **WA-23** | **15.2** | **33.5** | **3.47** | **13.8** | **2.84** | **0.63** | **3.18** | **0.46** | **2.80** | **15.0** | **0.55** | **1.65** | **0.23** | **1.58** | **0.24** | **95.14** | **1.09** | **1.27** | |
| FQ-26-R | 31.0 | 66.1 | 7.19 | 28.8 | 5.80 | 1.28 | 6.17 | 0.89 | 5.42 | 29.4 | 1.06 | 3.44 | 0.47 | 3.25 | 0.48 | 190.72 | 1.10 | 1.23 | M-H |
| FQ-26-1p | 28.0 | 59.9 | 6.24 | 24.9 | 4.79 | 1.02 | 5.10 | 0.68 | 3.99 | 19.7 | 0.76 | 2.35 | 0.32 | 2.32 | 0.34 | 160.41 | 1.09 | 1.26 | M-H |
| FQ-26-2c | 17.4 | 36.0 | 3.75 | 14.4 | 2.96 | 0.62 | 3.20 | 0.46 | 2.72 | 13.5 | 0.52 | 1.61 | 0.23 | 1.62 | 0.24 | 99.13 | 1.04 | 1.25 | M-H |
| FQ-26-3p | 24.2 | 48.5 | 5.21 | 20.2 | 4.03 | 0.82 | 4.22 | 0.59 | 3.51 | 18.4 | 0.69 | 2.12 | 0.31 | 2.18 | 0.32 | 135.30 | 1.03 | 1.23 | M-H |
| FQ-26-4p | 31.9 | 69.9 | 7.49 | 30.4 | 6.25 | 1.29 | 6.25 | 0.87 | 4.87 | 23.1 | 0.91 | 2.82 | 0.40 | 2.79 | 0.40 | 189.66 | 1.06 | 1.19 | M-H |
| FQ-26-5c | 19.0 | 43.1 | 4.46 | 17.8 | 3.69 | 0.81 | 4.14 | 0.62 | 3.77 | 19.6 | 0.76 | 2.31 | 0.32 | 2.34 | 0.34 | 123.02 | 1.06 | 1.25 | M-H |
| FQ-26-6c | 11.7 | 25.3 | 2.70 | 10.8 | 2.31 | 0.47 | 2.62 | 0.41 | 2.52 | 13.6 | 0.50 | 1.55 | 0.23 | 1.49 | 0.22 | 76.45 | 0.97 | 1.24 | H |
| FQ-26-7c | 6.3 | 33.2 | 1.43 | 5.51 | 0.99 | 0.14 | 1.10 | 0.13 | 0.72 | 2.69 | 0.13 | 0.38 | 0.06 | 0.39 | 0.06 | 53.16 | 0.72 | 1.35 | L-M |
| FQ-26-8c | 10.5 | 22.2 | 2.40 | 9.51 | 2.03 | 0.39 | 2.15 | 0.33 | 1.95 | 10.6 | 0.39 | 1.20 | 0.17 | 1.16 | 0.17 | 65.14 | 0.94 | 1.20 | M-H |
| FQ-26-9p | 21.6 | 46.5 | 4.92 | 19.6 | 4.36 | 1.02 | 4.97 | 0.78 | 4.98 | 29.0 | 1.05 | 3.21 | 0.45 | 3.04 | 0.45 | 146.05 | 1.11 | 1.25 | H |
| FQ-26-F | 31.0 | 69.9 | 7.25 | 29.5 | 6.15 | 1.43 | 6.72 | 0.94 | 5.68 | 28.6 | 1.11 | 3.16 | 0.46 | 3.16 | 0.46 | 195.43 | 1.16 | 1.26 | M-H |
| **WA-26** | **13.8** | **32.4** | **3.14** | **12.3** | **2.56** | **0.52** | **2.80** | **0.41** | **2.48** | **12.8** | **0.49** | **1.50** | **0.21** | **1.49** | **0.22** | **87.13** | **0.97** | **1.25** | |

REY, sum of rare earth elements and yttrium; values normalized by the average REY content of Upper Continent Crust (Taylor and McLennan, 1985) WA, weighted average (weighted by thickness of sample interval). The rows in bold are the weighted averages for each coal seam.

anomalies, slightly positive Ce and Eu anomalies, and weak negative Y anomalies (Fig. 8). The associated partings and floor and roof horizons of the No. 23 coal seam exhibit similar REY distribution patterns with those in the coal, but show more negative Y anomalies (Fig. 8).

All coal samples from the No. 26 seam exhibit similar REY distribution patterns (Fig. 8C), with the exception of the unusual sample FQ-26-7c, which has the highest $Ce_N/Ce_N^*$ value (2.53) and lowest $Eu_N/Eu_N^*$ value (0.72). The No. 26 Coal also has a distinct positive Gd anomalies and weak negative Y anomalies (Fig. 8C). The partings and roof and floor horizon samples from the No. 26 coal have distinct positive Gd anomalies, slight positive Ce and Eu anomalies, and weak negative Y anomalies (Fig. 8D).

## 5. Discussion

### 5.1. Sediment-source region

The $Al_2O_3/TiO_2$ ratio may stay almost unchanged during surface weathering and alteration of sedimentary deposits (Hayashi et al., 1997; He et al., 2010) indicating, in particular, the sediment-source regions for coal deposits (Hower et al., 2015b; Dai et al., 2015d, 2017). Typical $Al_2O_3/TiO_2$ ratios are 3–8, 8–21, and 21–70 for sediments derived from mafic, intermediate, and felsic igneous rocks, respectively (Hayashi et al., 1997).

With the exception of parting sample FQ-23-3p ($Al_2O_3/TiO_2$ = 20.8), the $Al_2O_3/TiO_2$ ratios for almost all the samples are higher than 21 (Fig. 9), indicating felsic compositions of the sediment-source region. A previous study by Dai et al. (2018) of the Baliancheng mine showed that terrigenous materials in the coal and its roof and floor horizons were dominantly derived from Mesozoic volcanic rocks. However, the Fuqiang coals in the present study are relatively rich in lithophile elements including Li, Rb, Zr, Ga, Pb, Sb, and, especially W, indicating some different terrigenous sediment sources between the Baliancheng and Fuqiang coals.

A comparison of the Fuqiang samples (coals, roofs, partings and floors) with the metamorphic and igneous rocks from the possible provenances (Zhang et al., 2006; Li et al., 2007; Guo et al., 2009; Liu et al., 2010; Ren et al., 2012; Chai et al., 2015; Chen et al., 2015, 2017; Li, 2017; Wu et al., 2017) is presented in Fig. 10 in terms of the Sr/Y, La/Yb, and $Al_2O_3/TiO_2$ ratios. Fig. 10 shows that the terrigenous materials for the samples of the Hunchun Basin were derived mainly from the Mesozoic (mostly Lower Cretaceous) intermediate-felsic volcanic rocks in addition to the Paleozoic crystalline rocks as previously suggested by Dai et al. (2018). Some Fuqiang samples show lower Sr/Y ratios relative to those of the Baliancheng mine samples (Fig. 10), indicating that the role of Paleozoic metamorphics (the Wudaogou Group) was probably higher for the samples of the Fuqiang mine than those of the Baliancheng mine. Metamorphic rocks of the Wudaogou Group are enriched in W, Pb, Sb, Cu, Zn and As (Chen et al., 2015; Li, 2017) in comparison with the averages for the continental crust in eastern China (Yan and Chi, 2005), and these metamorphic rocks mainly occur within the eastern Hunchun area and also provide the metallic materials for the W and Au mineralization (Chen et al., 2015). Thus, the Wudaogou Group and the Fuqiang coals and partings have similar Sr/Y and La/Yb ratios and elevated concentrations of elemental assemblage (e.g., W, Pb, and Sb). The paleogeography during deposition of coal-bearing sequences in the Hunchun Basin (Fig. 3) agrees with the input of the terrigenous materials from the metamorphic rocks surrounding the Hunchun Basin (Figs. 1C, 3).


**Fig. 8.** Distribution patterns of rare earth elements and yttrium in the Nos. 23 and 26 Coals. (A) and (B), No. 23 Coal; (C) and (D), No. 26 Coal. REY are normalized by Upper Continental Crust (UCC; Taylor and McLennan, 1985).

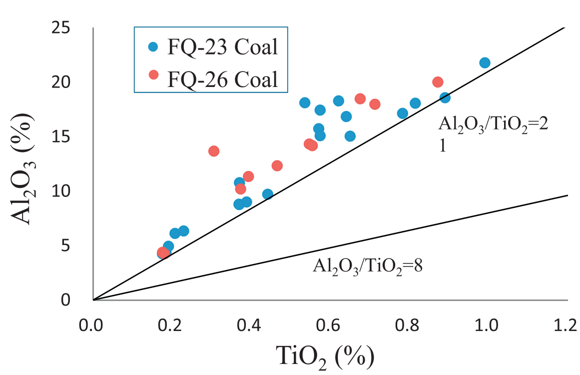


**Fig. 9.** Plot of $TiO_2$ vs. $Al_2O_3$ for the No. 23 and 26 Coals.

### 5.2. REY distribution

As described above, most samples of the Fuqiang coals are characterized by M- and H-type joint enrichment with a Gd-maximum. The study by Dai et al. (2018) shows that the Baliancheng coal has a similar Gd-maximum. This signature has not been found in any of the probable terrigenous rocks, but is well known for acidic natural waters, some of which circulated in coal basins (Johannesson and Zhou, 1997; Shand et al., 2005; Dai et al., 2014b, 2015b, 2015d, 2016c), as exemplified by the Late Permain coal of the Xinde Mine, Xuanwei, eastern Yunnan (Dai et al., 2014b) and the low-Ge coal of the Shengli Coalfield, northern China (Dai et al., 2015b). Although the M-type of REY enrichment in coal can also be caused by mafic volcanic ashes (Dai et al., 2015b, 2015d), no mafic contribution has been observed in the rocks of this study; instead, the $Al_2O_3/TiO_2$ ratio distinctly indicates a felsic source lithology.

Thus, in terms of REY distribution patterns of coals from the Hunchun Coalfield, both presented in this study and reported from the nearby Baliancheng mine by Dai et al. (2018), these coals appear to have been strongly subjected to acidic waters. This conclusion is also supported by elevated concentrations of B in the Fuqiang and Baliancheng coals (86 and 92 μg/g on average, respectively). The concentrations and correlation coefficients between B and ash yields in the Fuqiang coals (−0.75) and Baliancheng coal (−0.73, Dai et al., 2018) indicate that B was derived from acidic waters. A similar source of B in lignite has been reported by Dai et al. (2015b) in the Shengli Coalfield, northern China. Although the elevated concentration of B in coal can be caused by marine influence (Goodarzi and Swaine, 1994), precipitated from hydrothermal solutions (Lyons et al., 1989), or derived from volcanic activity (Bouška and Pešek, 1983; Karayigit et al., 2000), no evidence for these factors has been identified in the Fuqiang and Baliancheng coals.

In addition to a mafic rocks in the terrigenous region, the highly positive Eu anomalies in coal could be caused by extremely reducing conditions coupled with high-temperatures (e.g., > 250 °C, Sverjensky, 1984), which do not appear within natural aquatic systems (Bau, 1991; Dai et al., 2016b). Dai et al. (2018) shows that the weak anomalies of positive Eu in the Baliancheng coal ($Eu_N/Eu_N^* = 1.19$ on average) were inherited from the source rocks. The weak positive Eu anomalies in the Fuqiang coals (except sample FQ-26-7c) were probably related to the Paleozoic metamorphic rocks, some of which also display positive Eu anomalies (Chen et al., 2015; Li, 2017).

In contrast to the other samples, sample FQ-26-7c has a distinct positive Ce anomaly (Fig. 8C), This indicates that the coal bench has been subjected to strong leaching under oxidizing conditions, which is supported by the highest clay concentration in the low temperature-ash of this sample (~93.7%), relatively high contents of resistant elements such as Zr and Ga (Fig. 7), and a high ash yield of this bench. It may be speculated that the coal or its parent peat was exposed to the Earth's surface oxidizing conditions for a relatively long time and consequently

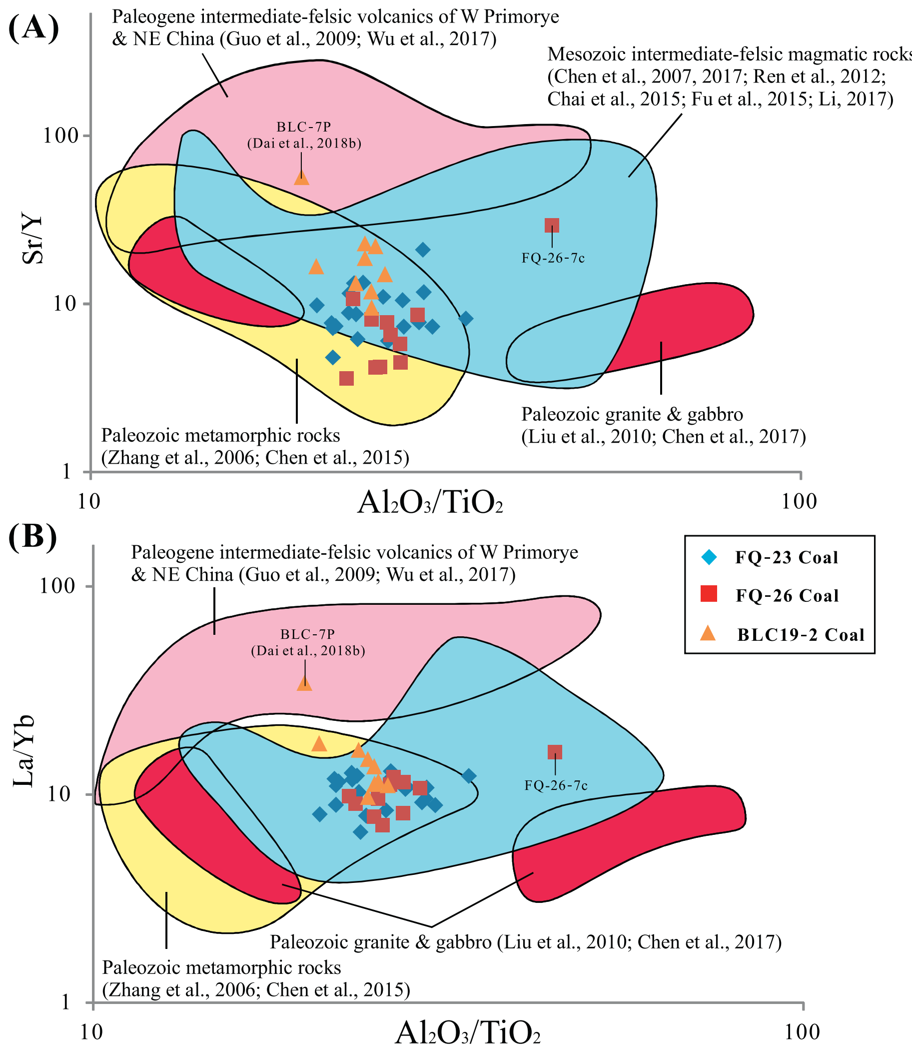


**Fig. 10.** Comparison between the studied samples (including Dai et al., 2018) and their possible magmatic and metamorphic source rocks with the $Al_2O_3/TiO_2$ vs. Sr/Y and La/Yb (modified after Dai et al., 2018).

resulted in strong leaching. During exposure of the ply of coal/peat to aerobic leaching process, $Ce^{3+}$ was oxidized to $Ce^{4+}$, which is usually immobile and is preferentially precipitated in-situ (Braun et al., 1990; De Carlo et al., 1998; Taunton et al., 2000). This leaching process leads to the generation of Ce-poor REY-rich leachates from the coal/peat ply, and results in low total REY content, and consequently high Ce content and $Ce_N/Ce_N^*$ values in the in-situ coal/peat ply.

The negative Y anomalies, which occur in almost all of the studied rocks, especially partings, roofs, and floors (Fig. 8), probably reflect significant leaching of this element from the lower coal-bearing unit of the Hunchun basin. Dai et al. (2018) also showed the similar negative Y anomalies in the Baliancheng coal. This might result in its redeposition at the artesian-water discharge zones along faults cutting and framing the basin. This phenomenon was observed in South Primorye (Nechaev et al., 2018).

### 5.3. Relationship between Hunchun coals and adjacent ore deposits

Mineralization is common in the eastern Jilin Province of NE China (Ren et al., 2016; Chen et al., 2017) and several Au–Cu and W deposits were discovered in this area. The Paleozoic low-grade metamorphic rocks (mainly the Wudaogou Group), Permain granitoids and Mesozoic (mainly Early Cretaceous) magmatic rocks are important host rocks for the ore mineralization in the eastern Hunchun area (Chen et al., 2015, 2017; Ren et al., 2016). These rocks also served as sediment-source rocks for the Paleogene coal-bearing sediments in the Hunchun Coalfield as shown in this study and the investigation by Dai et al. (2018). It is noteworthy that many of the ore deposits are situated nearer to the Fuqiang coal mine than to the Baliancheng coal mine (Fig. 1). Mineralization of Yangjingou and Wudaogou scheelite deposits (Zhang et al., 2006; Li, 2017) in the Paleozoic rocks in Eastern Jilin is a probable reason for the W enrichment in the Fuqiang samples.

The geological setting, which led to the trace element enrichment in coals in the Hunchun Coalfield, probably included the following processes:

1) W-mineralized igneous and metamorphic rocks surrounding the coal basin have been subjected to weathering and erosion after tectonic uplift, and subsequently provided sheelite and other ore components as solid particles and dissolved elements and compounds into the coal basin by stream and ground waters, particularly by those with $pH > 8$ (e.g., Grimes et al., 1995; Johannesson et al., 2013).
2) The ore detrital particles or the leached elements were deposited in the peat deposit layers and their adjacent non-peat host sediments in the coal basin, which served as geochemical barriers of the groundwater aquifer in the basin. The acidic environment during peat deposition as evidenced by the REY's distribution could facilitate the deposition of ore detrital particles and leached elements.

## 6. Conclusions

The Fuqinag coals (Nos. 23 and 26) from the Hunchun Coalfield have low random huminite reflectances (0.31–0.49%) and are rich in W, Cs, Rb, and some other lithophyte elements (Li, V, Ga, and Zr). The terrigenous regions for the coals are Mesozoic intermediate-felsic volcanic rocks and Paleozoic low-grade metamorphic (mainly the Wudaogou Group) and magmatic rocks.

The coals of the Hunchun Coalfiled are rich in tungsten and may be classified as 'coal-hosted rare-metal deposit' or 'metalliferous coal' with related potential economic value. These characteristics are due to their proximity to the eastern Hunchun ore district, where gold and tungsten mineralizations are abundant.

## Acknowledgments

This research was supported by the National Natural Science Foundation of China (No. 41420104001), the 111 Project (no. B17042), the Program for Changjiang Scholars and Innovative Research Team in University (No. IRT_17R104), the Yue Qi Scholar Project, and the Far Eastern Branch, Russian Academy of Sciences (Grant No. 18-2-020).

## References

ASTM D3173/D3173M-17a, 2017. Standard Test Method for Moisture in the Analysis Sample of Coal and Coke. ASTM International, West Conshohocken, PA. www.astm.org.
ASTM D3174-12, 2012. Standard Test Method for Ash in the Analysis Sample of Coal and Coke from Coal. ASTM International, West Conshohocken, PA. www.astm.org.
ASTM D3175-17, 2017. Standard Test Method for Volatile Matter in the Analysis Sample of Coal and Coke. ASTM International, West Conshohocken, PA. www.astm.org.
ASTM Standard D2798-11a, 2011. Test Method for Microscopical Determination of the Vitrinite Reflectance of Coal. ASTM International, West Conshohocken, PA.
ASTM Standard D3177-02, 2011. Test Methods for Total Sulfur in the Analysis Sample of Coal and Coke. ASTM International, West Conshohocken, PA.
ASTM Standard D388-12, 2012. Standard Classification of Coals by Rank. ASTM International, West Conshohocken, PA.
ASTM Standards D5865-13, 2013. Standard Test Method for Gross Calorific Value of Coal and Coke. ASTM International, West Conshohocken, PA.
ASTM Standards D5987-96, 2015. Standard Test Method for Total Fluorine in Coal and Coke by Pyrohydrolytic Extraction and Ion Selective Electrode or Ion Chromatograph Methods. ASTM International, West Conshohocken, PA.
Bau, M., 1991. Rare-earth element mobility during hydrothermal and metamorphic fluidrock interaction and the significance of the oxidation state of europium. Chem. Geol. 93, 219–230.
Bouška, V., Pešek, J., 1983. Boron in the aleuropelites of the Bohemian massif. In: 5th Meet. Europ. Clay Groups (Prague), pp. 147–155.
Braun, J.-J., Pagel, M., Muller, J.-P., Bilong, P., Michard, A., Guillet, B., 1990. Cerium anomalies in lateritic profiles. Geochim. Cosmochim. Acta 54, 781–795.
Cao, H., Xu, W., Pei, F., Zhang, X., 2011. Permian tectonic evolution in Southwestern Khanka Massif: Evidence from zircon U-Pb chronology, Hf isotope and geochemistry of gabbro and diorite. Acta Geol. Sin. 85, 1390–1402.
Chai, P., Sun, J., Xing, S., Men, L., Han, J., 2015. Early Cretaceous arc magmatism and high-sulphidation epithermal porphyry Cu-Au mineralization in Yanbian area, Northeast China: the Duhuangling example. Int. Geol. Rev. 57, 1267–1293.
Chen, C., Ren, Y., Zhao, H., Zou, X., Yang, Q., Hu, Z., 2014. Permian age of the Wudaogou Group in eastern Yanbian: detrital zircon U-Pb constrains on the closure of the Palaeo-Asian Ocean in Northeast China. Int. Geol. Rev. (14), 1754–1768.
Chen, C., Ren, Y., Zhao, H., Yang, Q., Zou, X., 2015. The whole-Rock geochemical composition of the Wudaogou Group in eastern Yanbian, NE China-New clues to its relationship with the gold and tungsten mineralization and the evolution of the Paleo-Asian Ocean. Resour. Geol. 65, 232–248.
Chen, C., Ren, Y., Zhao, H., Yang, Q., Shang, Q., 2017. Age, tectonic setting, and metallogenic implication of Phanerozoic granitic magmatism at the eastern margin of the Xing'an–Mongolian Orogenic Belt, NE China. J. Asian Earth Sci. 144, 368–383.
Chinese Standard Method GB/T 15224.1-2010, 2010. Classification for Quality of Coal. Part 1: Ash, Standardization Administration of China. Coal Analysis Laboratory of China Coal Research Institute, Beijing, China (in Chinese).
Chou, C.-L., 2012. Sulfur in coals: A review of geochemistry and origins. Int. J. Coal Geol. 100, 1–13.
Dai, S., Finkelman, R.B., 2018. Coal as a promising source of critical elements: progress and future prospects. Int. J. Coal Geol. 186, 155–164.
Dai, S., Wang, X., Seredin, V.V., Hower, J.C., Ward, C.R., O'Keefe, J.M.K., Huang, W., Li, T., Li, X., Liu, H., Xue, W., Zhao, L., 2012a. Petrology, mineralogy, and geochemistry of the Ge-rich coal from the Wulantuga Ge ore deposit, Inner Mongolia, China: new data and genetic implications. Int. J. Coal Geol. 90-91, 72–99.
Dai, S., Ren, D., Chou, C.-L., Finkelman, R.B., Seredin, V.V., Zhou, Y., 2012b. Geochemistry of trace elements in Chinese coals: a review of abundance, genetic types, impacts on human health, and industrial utilization. Int. J. Coal Geol. 94, 3–21.
Dai, S., Song, W., Zhao, L., Li, X., Hower, J.C., Ward, C.R., Wang, P., Li, T., Zheng, X., Seredin, V.V., Xie, P., Li, Q., 2014a. Determination of boron in coal using closed-vessel microwave digestion and inductively coupled plasma mass spectrometry (ICP-MS). Energy Fuel 28, 4517–4522.
Dai, S., Li, T., Seredin, V.V., Ward, C.R., Hower, J.C., Zhou, Y., Zhang, M., Song, X., Song, W., Zhao, C., 2014b. Origin of minerals and elements in the Late Permian coals, tonsteins, and host rocks of the Xinde Mine, Xuanwei, eastern Yunnan, China. Int. J. Coal Geol. 121, 53–78.
Dai, S., Wang, P., Ward, C.R., Tang, Y., Song, X., Jiang, J., Hower, J.C., Li, T., Seredin, V.V., Wagner, N.J., Jiang, Y., Wang, X., Liu, J., 2015a. Elemental and mineralogical anomalies in the coal-hosted Ge ore deposit of Lincang, Yunnan, southwestern China: Key role of $N_2$-$CO_2$-mixed hydrothermal solutions. Int. J. Coal Geol. 152, 19–46.
Dai, S., Liu, J., Ward, C.R., Hower, J.C., Xie, P., Jiang, Y., Hood, M.M., O'Keefee, J.M.K., Song, H., 2015b. Petrological, geochemical, and mineralogical compositions of the low-Ge coals from the Shengli Coalfield, China: a comparative study with Ge-rich coals and a formation model for coal-hosted Ge ore deposit. Ore Geol. Rev. 71, 318–349.
Dai, S., Seredin, V.V., Ward, C.R., Hower, J.C., Xing, Y., Zhang, W., Song, W., Wang, P., 2015c. Enrichment of U-Se-Mo-Re-V in coals preserved within marine carbonate successions: geochemical and mineralogical data from the Late Permian Guiding Coalfield, Guizhou, China. Mineral. Deposita 50, 159–186.
Dai, S., Li, T., Jiang, Y., Ward, C.R., Hower, J.C., Sun, J., Liu, J., Song, H., Wei, J., Li, Q., Xie, P., Huang, Q., 2015d. Mineralogical and geochemical compositions of the Pennsylvanian coal in the Hailiushu Mine, Daqingshan Coalfield, Inner Mongolia, China: implications of sediment-source region and acid hydrothermal solutions. Int. J. Coal Geol. 137, 92–110.
Dai, S., Chekryzhov, I.Y., Seredin, V.V., Nechaev, V.P., Graham, I.T., Hower, J.C., Ward, C.R., Ren, D., Wang, X., 2016a. Metalliferous coal deposits in East Asia (Primorye of Russia and South China): a review of geodynamic controls and styles of mineralization. Gondwana Res. 29, 60–82.
Dai, S., Graham, I.T., Ward, C.R., 2016b. A review of anomalous rare earth elements and yttrium in coal. Int. J. Coal Geol. 159, 82–95.
Dai, S., Liu, J., Ward, C.R., Hower, J.C., French, D., Jia, S., Hood, M.M., Garrison, T.M., 2016c. Mineralogical and geochemical compositions of Late Permian coals and host rocks from the Guxu Coalfield, Sichuan Province, China, with emphasis on enrichment of rare metals. Int. J. Coal Geol. 166, 71–95.
Dai, S., Ward, C.R., Graham, I.T., French, D., Hower, J.C., Zhao, L., Wang, X., 2017. Altered volcanic ashes in coal and coal-bearing sequences: A review of their nature and significance. Earth-Sci. Rev. 175, 44–74.
Dai, S., Guo, W., Nechaev, V.P., French, D., Ward, C.R., Spiro, B.F., Finkelman, R.B., 2018. Modes of occurrence and origin of mineral matter in the Palaeogene coal (No. 19-2) from the Hunchun Coalfield, Jilin Province, China. Int. J. Coal Geol. 189, 94–110.
De Carlo, E.H., Wen, X.-Y., Irving, M., 1998. The influence of redox reactions on the uptake of dissolved Ce by suspended Fe and Mn oxide particles. Aquat. Geochem. 3, 357–389.
Donskaya, T.V., Gladkochub, D.P., Mazukabzov, A.M., Ivanov, A.V., 2012. Late Paleozoic-Mesozoic subduction-related magmatism at the southern margin of the Siberian continent and the 150 million-year history of the Mongol-Okhotsk Ocean. J. Asian Earth Sci. 62, 79–97.
Finkelman, R.B., Palmer, C.A., Wang, P., 2017. Quantification of the modes of occurrence of 42 elements in coal. Int. J. Coal Geol. 185, 138–160.
Goodarzi, F., Swaine, D.J., 1994. Paleoenvironmental and environmental implications of the boron content of coals. Geol. Surv. Can. Bull. 471, 1–46.
Grigoriev, N.A., 2009. Chemical Element Distribution in the Upper Continental Crust. UB RAS, Ekaterinburg, pp. 382 (in Russian).
Grimes, D.J., Ficklin, W.H., Meier, A.L., McHugh, J.B., 1995. Anomalous gold, antimony, arsenic, and tungsten in ground water and alluvium around disseminated gold deposits along the Getchell Trend, Humboldt County, Nevada. J. Geochem. Explor. 52, 351–371.
Guo, F., Nakamura, E., Fan, W., Kobayashi, K., Li, C., Guo, X., 2009. Mineralogical and geochemical constraints on magmatic evolution of Paleocene adakitic andesites from the Yanji area, NE China. Lithos 112, 321–341.
Hayashi, K.I., Fujisawa, H., Holland, H.D., Ohmoto, H., 1997. Geochemistry of ~1.9 Ga sedimentary rocks from northeastern Labrador, Canada. Geochim. Cosmochim. Acta 61, 4115–4137.
He, B., Xu, Y., Zhong, Y., Guan, J., 2010. The Guadalupian–Lopingian boundary mudstones at Chaotian (SW China) are clastic rocks rather than acidic tuffs: implication for a temporal coincidence between the end-Guadalupian mass extinction and the Emeishan volcanism. Lithos 119, 10–19.
Hower, J.C., Groppo, J.G., Henke, K.R., Hood, M.M., Eble, C.F., Honaker, R.Q., Zhang, W., Qian, D., 2015a. Notes on the potential for the concentration of rare earth elements and yttrium in coal combustion fly ash. Minerals 5, 356–366.
Hower, J.C., Eble, C.F., O'Keefe, J.M.K., Dai, S., Wang, P., Xie, P., Liu, J., Ward, C.R., French, D., 2015b. Petrology, palynology, and geochemistry of Gray Hawk Coal (Early Pennsylvanian, Langsettian) in Eastern Kentucky, USA. Minerals 5, 592–622.
Johannesson, K.H., Zhou, X., 1997. Geochemistry of the rare earth element in natural terrestrial waters: a review of what is currently known. Chin. J. Geochem. 16, 20–42.
Johannesson, K.H., Dave, H.B., Mohajerin, T.J., Datta, S., 2013. Controls on tungsten concentrations in groundwater flow systems: The role of adsorption, aquifer sediment Fe (III) oxide/oxyhydroxide content, and thiotungstate formation. Chem. Geol. 351, 76–94.
Karayigit, A.I., Gayer, R.A., Querol, X., Onacak, T., 2000. Contents of major and trace elements in feed coals from Turkish coal-fired power plants. Int. J. Coal Geol. 44, 169–184.
Ketris, M.P., Yudovich, Ya.E., 2009. Estimations of Clarkes for carbonaceous biolithes:

world average for trace element contents in black shales and coals. Int. J. Coal Geol. 78, 135–148.
Li, C., 2017. Analyses on the Geological Characteristics and Exploration Perspective of Wudaogou Tungsten Deposit, Jilin Province (Ms. Thesis). Jilin University (61 pp. (in Chinese)).
Li, C., Guo, F., Fan, W., Guo, X., 2007. Ar-Ar geochronology of Late Mesozoic volcanic rocks from the Yanji area, NE China and tectonic implications. Sci. China Ser. D Earth Sci. 50 (4), 505–518.
Li, X., Dai, S., Zhang, W., Li, T., Zheng, X., Chen, W., 2014. Determination of As and Se in coal and coal combustion products using closed vessel microwave digestion and collision/reaction cell technology (CCT) of inductively coupled plasma mass spectrometry (ICP-MS). Int. J. Coal Geol. 124.
Liu, S., Hu, R., Gao, S., Feng, C., Feng, G., Coulson, I.M., Li, C., Wang, T., Qi, Y., 2010. Zircon U–Pb age and Sr–Nd–Hf isotope geochemistry of Permian granodiorite and associated gabbro in the Songliao Block, NE China and implications for growth of juvenile crust. Lithos 11, 423–436.
Liu, J., Ward, C.R., Graham, I.T., French, D., Dai, S., Song, X., 2018. Modes of occurrence of non-mineral inorganic elements in lignites from the Mile Basin, Yunnan Province, China. Fuel 222, 146–155.
Lyons, P.C., Palmer, C.A., Bostick, N.H., Fletcher, J.D., Dulong, F.T., Brown, F.W., Brown, Z.A., Krasnow, M.R., Romankiw, L.A., 1989. Chemistry and origin of minor and trace elements in vitrinite concentrates from a rank series from the eastern United States, England, and Australia. Int. J. Coal Geol. 13, 481–527.
Medvedev, Ya.V., Sedykh, A.K., Chelpanov, V.A., 1997. Pavlovsk Deposit. Coal Resources of Russia, V-I. Geoinformmark, Moscow, pp. 175–194 (in Russian).
Moon, J.-W., Moon, H.-S., Woo, N.-C., Hahn, J.-S., Won, J.-S., Song, Y., Lin, X., Zhao, Y., 2000. Evaluation of heavy metal contamination and implication of multiple sources from Hunchun basin, northeastern China. Environ. Geol. 39, 1039–1052.
Nechaev, V.P., Chekryzhov, I.Yu., Vysotskiy, S.V., Ignatiev, A.V., Velivetskaya, T.A., Tarasenko, I.A., Agoshkov, A.I., 2018. Isotopic signatures of REY mineralization associated with lignite basins in South Primorye, Russian Far East. Ore Geol. Rev. https://doi.org/10.1016/j.oregeorev.2018.01.018.
Qi, H., Hu, R., Zhang, Q., 2007. REE geochemistry of the Cretaceous lignite from Wulantuga Germanium Deposit, Inner Mongolia, Northeastern China. Int. J. Coal Geol. 71, 329–344.
Qin, S., Lu, Q., Li, Y., Wang, J., Zhao, Q., Gao, K., 2018. Relationships between trace elements and organic matter in coals. J. Geochem. Explor. 188, 101–110.
Ren, Y., Ju, N., Zhao, H., Wang, H., Hou, K., Liu, S., 2012. Geochronology and geochemistry of metallogenetic porphyry bodies from the Nongping Au-Cu deposit in the eastern Yanbian area, NE China: implications for metallogenic environment. Acta Geol. Sin. (English Ed.) 86, 619–629.
Ren, Y., Chen, C., Zou, X., Zhao, H., Hao, Y., Hou, H., Hu, Z., Jiang, G., 2016. The age, geological setting, and types of gold deposits in the Yanbian and adjacent areas, NE China. Ore Geol. Rev. 73, 284–297.
Seredin, V.V., Dai, S., 2012. Coal deposits as potential alternative sources for lanthanides and yttrium. Int. J. Coal Geol. 94, 67–93.
Seredin, V.V., Danilcheva, J., 2001. Coal-hosted Ge deposits of the Russian Far East. In: Piestrynsky, A. (Ed.), Mineral Deposits at the Beginning of the 21st Century. Swets & Zeitlinger Publishers, Lisse, The Netherlands, pp. 89–92.
Seredin, V.V., Finkelman, R.B., 2008. Metalliferous coals: a review of the main genetic and geochemical types. Int. J. Coal Geol. 76, 253–289.
Seredin, V.V., Danilcheva, Yu.A., Magazina, L.O., Sharova, I.G., 2006. Ge-bearing coals of the Luzanovka Graben, Pavlovka brown coal deposit, Southern Primorye. Lithol. Miner. Resour. 41, 280–301.
Shand, P., Johannesson, K.H., Chudaev, O., Chudaeva, V., Edmunds, W.M., 2005. Rare earth element contents of high pCO2 groundwaters of Primorye, Russia: mineral stability and complexation controls. In: Johannesson, K.H. (Ed.), Rare Earth Elements in Groundwater Flow System. Springer, The Netherlands, pp. 161–186.
Sun, J., 2015. Discussion on coal-bearing strata and coal accumulation pattern in Yili coalfield, Hunchun Basin. Sci. Technol. Innov. 28, 107 (In Chinese).
Sun, J., Chen, L., Zhao, J., Men, L., Pang, W., Chen, D., Liang, S., 2008. SHRIMP U-Pb dating of zircons from Late Yanshanian granitic complex in Xiaoxi'nancha gold-rich copper ore field of Yanbian and its geological implications. Mineral Deposits 27, 319–328 (In Chinese with English abstract).
Sun, Y., Li, M., Ge, W., Zhang, Y., Zhang, D., 2013. Eastward termination of Solonker-Xar Moron River Suture determined by detrital zircon U-Pb isotopic dating and Permian floristics. J. Asian Earth Sci. 75, 243–250.
Sverjensky, D.A., 1984. Europium redox equilibria in aqueous solution. Earth Planet. Sci. Lett. 67, 70–78.
Taunton, A.E., Welch, S.A., Banfield, J.F., 2000. Microbial controls on phosphate and lanthanide distributions during granite weathering and soil formation. Chem. Geol. 169, 71–382.
Taylor, S.R., McLennan, S.H., 1985. The Continental Crust: Its Composition and Evolution. Blackwell, Oxford (312 pp.).
Wang, Y., 2015. Low rank enrichment of coalbed methane in Hunchun basin. Coal Geol. Exp. 43 (3), 28–32 (in Chinese with English abstract).
Wang, J., Wang, B., 2004. The underlying coal-bearing member deposition of Hunchun coalfield and its concentrating coal characteristics. Jilin Geol. 23 (2), 21–27 (in Chinese with English abstract).
Wang, Y., Wei, P., Shi, J., 2009. Ore-forming geological conditions and prospecting direction of Au-Cu-W ore belt of eastern part of Hunchun, Jilin Province. Jilin Geol. 28 (3), 35–38 (in Chinese with English abstract).
Ward, C.R., Matulis, C.E., Taylor, J.C., Dale, L.S., 2001. Quantification of mineral matter in the Argonne Premium coals using interactive Rietveld-based X-ray diffraction. Int. J. Coal Geol. 46, 67–82.
Wen, Y., 2014. Analysis of coal accumulation environment in Hunchun Coalfield. West-China Explor. Eng. 26 (9), 159–160 (in Chinese).
Wu, F., Jahn, B.M., Wilde, S., Sun, D., 2000. Phanerozoic crustal growth: U-Pb and Sr-Nd isotopic evidence from the granites in northeastern China. Tectonophysics 328, 89–113.
Wu, F., Sun, D., Li, H., Jahn, B.M., Wilde, S.A., 2002. A-type granites in northeastern China: age and geochemical constrains on their petrogenesis. Chem. Geol. 187, 143–173.
Wu, F., Zhao, G., Sun, D., Wilde, S.A., Yang, J., 2007. The Hulan Group: its role in the evolution of the Central Asian Orogenic Belt of NE China. J. Asian Earth Sci. 30, 542–556.
Wu, F., Sun, D., Ge, W., Zhang, Y., Grant, M.L., Wilde, S.A., Jahn, B.M., 2011. Geochronology of the Phanerozoic granitoids in northeastern China. J. Asian Earth Sci. 41, 1–30.
Wu, T.J., Jahn, B.M., Nechaev, V., Chashchin, A., Popov, V., Yokoyama, K., Tsutsumi, Y., 2017. Geochemical characteristics and petrogenesis of adakites in the Sikhote-Alin area, Russian Far East. J. Asian Earth Sci. 145, 512–529.
Xu, X., Han, Z., 1990. The genetic types of the Paleogene volcaniclastic rock in Hunchun. J. Shangdong Ming Inst. 1, 43–50 (in Chinese with English abstract).
Xu, W., Pei, F., Wang, F., Meng, E., Ji, W., Yang, D., Wang, W., 2013. Spatial-temporal relationships of Mesozoic volcanic rocks in NE China: constraints on tectonic overprinting and transformations between multiple tectonic regimes. J. Asian Earth Sci. 74, 167–193.
Yan, M., Chi, Q., 2005. The Chemical Compositions of the Continental Crust and Rocks in the Eastern Part of China. Science Press, Beijing (171 pp.).
Yang, D.-G., Sun, D.-Y., Hou, X.-G., Mao, A.-Q., Tang, Z.-Y., Qin, Z., 2018. Geochemistry and zircon Hf isotopes of the Early Mesozoic intrusive rocks in the south Hunchun, Yanbian area, Northeast China: petrogenesis and implications for crustal growth. Int. Geol. Rev. 60, 1038–1060.
Zhang, Y., Wu, F., Wilde, S.A., Zhai, M., Lu, X., Sun, D.Y., 2004. Zircon U-Pb ages and tectonic implications of 'Early Paleozoic' granitoids at Yanbian, Jilin Province, northeast China. Island Arc 13, 484–505.
Zhang, H., Wang, J., Fu, S., Ai, X., 2006. Wallrock alteration and mass transfer regularity in the Yangjingou scheelite deposit. Geol. Prospect. 42 (5), 1–7 (in Chinese with English abstract).
Zhang, J., Gao, S., Ge, W., Wu, F., Yang, J., Wilde, S.A., Li, M., 2010. Geochronology of the Mesozoic volcanic rocks in the Great Xing'an Range, northeastern China: implications for subduction-induced delamination. Chem. Geol. 276, 144–165.
Zhao, Y., Sun, J., Wang, Q., Men, L., Li, Y., Guo, J., 2010. $^{40}Ar/^{39}Ar$ laser probe dating and discussion on metallogenic epoch of epithermal Au-Cu deposit in Yanbian area of Jilin. Earth Sci. Front. 17 (2), 156–169 (in Chinese with English abstract).
Zhao, H., Ren, Y., Hou, H., Wang, H., Ju, N., Chen, C., Li, C., 2013. Metallogenic age and tectonic setting of the first orogenic gold deposit discovered in the Yanbian region, NE China. Int. Geol. Rev. 55 (7), 882–893.